Double occupancy of the f orbital in the Anderson model for Ce compounds

O. Gunnarsson
Max-Planck-Institut für Festkörperforschung, D-7000 Stuttgart 80, West Germany

K. Schönhammer*
I. Institut für Theoretische Physik, Universität Hamburg, D-2000 Hamburg 36, West Germany
(Received 30 July 1984)

The Anderson model at zero temperature is studied as a function of the f-level position ε_f and the f-level—conduction-electron hopping matrix element V. The f-f Coulomb interaction U is assumed to be finite, and double occupancy of the f level is taken into account. For a large value of the f-level degeneracy N_f, there is an important asymmetry between f^0 and f^2 configurations. Even for "symmetric" parameters, $2\varepsilon_f+U=2\varepsilon_F=0$, the f^2 weight is much larger than the f^0 weight if V is small. The effect of this asymmetry on other properties is studied for $N_f\to\infty$. The static susceptibility is primarily determined by the f^0 weight, while the shape of the valence photoemission spectrum close to the Fermi energy ε_F also has an important dependence on the f^2 weight. The valence photoemission spectrum can have a pronounced two-peak character, with one peak close to ε_f and a second structure close to ε_F. For ε_f well below ε_F ("spin-fluctuation" limit) the weight of the second structure can be strongly enhanced compared to the $U=\infty$ limit, and its shape and position depends on the conduction density of states. This structure can therefore have a peak below ε_F. The bremsstrahlung isochromat spectroscopy spectrum shows an f^1 peak with an energy separation from ε_F which is determined by the "Kondo" temperature. The tail of this peak contributes to the structure in the valence photoemission spectrum below ε_F. Ground-state properties are calculated variationally, treating $1/N_f$ as a small parameter. A new technique for performing these calculations is developed. This technique makes it possible to include such a large basis set that accurate results are obtained for the ground-state energy and the f-level occupancy in the limit $N_f=1$. To calculate the spectra we introduce a time-dependent method which facilitates the inclusion of f^2 configurations in the valence photoemission spectrum.

I. INTRODUCTION

Ce mixed-valence compounds are often described by the Anderson model.[1] Traditionally, it has been assumed that the f^0 and f^1 configurations are almost degenerate and much lower in energy than the f^2 configuration. The Anderson model has therefore often been studied in the limit where the Coulomb interaction U between two f electrons is infinite and the f^2 configurations are entirely suppressed. The Bethe ansatz[2] has, for instance, been used to calculate certain properties of the Anderson model exactly in the limit $U=\infty$ for an infinitely broad and structureless conduction band.[3] These calculations have been performed for different values of the degeneracy N_f of the f level. Recently, there have been strong indications[4–7] that the f^1 configuration may be a few electron volts lower than the f^0 configuration. Since U is of the order of 5–6 eV,[5] the energy of the f^0 and f^2 configurations are then comparable, and the assumption $U=\infty$ is not really justified for these systems. The thermodynamic properties of the Anderson model for a finite U and $N_f=2$ have been studied extensively using the renormalization-group technique[8] or the Bethe ansatz.[9] In a recent paper,[10] referred to hereafter as paper I, we found that the extension to $N_f>2$ leads to many new features. The aim of this paper is therefore to study both the ground-state and spectroscopic properties of the Anderson model at $T=0$ for a finite U and a large N_f. We consider the Anderson impurity Hamiltonian[1]

$$H=\sum_{\nu=1}^{N_f}\left[\int\varepsilon\psi_{\varepsilon\nu}^{\dagger}\psi_{\varepsilon\nu}d\varepsilon+\varepsilon_f\psi_{\nu}^{\dagger}\psi_{\nu}+\int d\varepsilon[V(\varepsilon)\psi_{\nu}^{\dagger}\psi_{\varepsilon\nu}+\text{H.c.}]\right]+U\sum_{\substack{\nu,\mu\\ \nu<\mu,}}n_{\nu}n_{\mu}\ . \tag{1.1}$$

We have introduced a combined index, ν, for the orbital and spin degeneracies. The spin-orbit and multiplet splittings are neglected. The first term describes the conduction states, with energies ε, and the second term the f level with the (bare) energy ε_f. The third term leads to hopping between these states and the last term includes the Coulomb interaction between the f electrons. As was discussed in paper I, Eq. (1.1) is obtained from the normal form of the Anderson model by a linear transformation of the conduction states. This transformation also leads to states which do not couple to the f level and which are therefore not included. In $V(\varepsilon)$, a factor $\sqrt{\rho(\varepsilon)}$ is absorbed, where $\rho(\varepsilon)$ is the conduction density of states. In the following we set the Fermi energy equal to zero, $\varepsilon_F=0$. The special choice $2\varepsilon_f+U=0$ has been given particular attention for $N_f=2$ and a symmetric choice of $V(\varepsilon)$ around ε_F. This so-called symmetric Anderson model has electron-hole symmetry and the f^0 and f^2 con-

figurations have equal weight. For $N_f > 2$ the electron-hole—pair symmetry is lost, even for a "symmetric" choice of the parameters. To study this we present an exact solution for the limit of an infinite N_f. This solution shows that the f^2 weight can be much larger than the f^0 weight, even for $2\varepsilon_f + U = 0$ and a "symmetric" $V(\varepsilon)$. The aim of this paper is to study further the influence of the f^0 and f^2 weights on various properties, such as the ground-state energy, the magnetic susceptibility, and the valence photoemission spectrum. We find that the inclusion of f^2 states leads to important effects for the photoemission spectrum and that, in contrast to the $N_f = 2$ case, the susceptibility is mainly determined by the f^0 weight.

In Sec. II we present a new method for calculating ground-state properties, treating $1/N_f$ as a small parameter.[11] The idea that $1/N_f$ is a small quantity has earlier been used to calculate ground-state properties.[10–13] In paper I we developed a method for calculating spectroscopic properties for $U = \infty$ and, to a certain extent, for $U < \infty$ as well. Alternative methods for obtaining spectra were later developed for $U = \infty$ and $T \geq 0$.[13] In Sec. III we test the accuracy of this method for finite N_f by comparison with exact results for $N_f = 1$ and, to some extent, for $N_f = 2$. In Sec. IV we study some ground-state properties, in particular the f^0 and f^2 weights and the susceptibility. In Sec. V a new method for calculating the valence photoemission and the bremsstrahlung isochromat spectra (BIS) is presented, and the interference between transitions involving f and conduction electrons is discussed.

II. GROUND-STATE PROPERTIES

In this section we extend the method used in paper I for calculating some ground-state properties, with particular focus on cases where the f-level degeneracy N_f is large. The quantity $1/N_f$ can then be considered a small parameter.[11] To see this we study the limit of large N_f with the subsidary condition

$$\sqrt{N_f} V(\varepsilon) \equiv \tilde{V}(\varepsilon) , \tag{2.1}$$

where $\tilde{V}(\varepsilon)$ is independent of N_f, which allows us to choose basis states in a systematic way. This is indicated in Fig. 1. Since the ground state is a singlet (for $N_f = 2$),[8] we only consider singlet basis states. We introduce

$$|0\rangle = \prod_{\nu=1}^{N_f} \prod_{\varepsilon \leq \varepsilon_F} \psi^\dagger_{\varepsilon\nu} |\,\text{vacuum}\rangle , \tag{2.2}$$

with the f level empty and all conduction states below the Fermi energy, $\varepsilon_F = 0$, filled. We have used the normalization

$$\{\psi_{\varepsilon\nu}, \psi^\dagger_{\varepsilon'\nu'}\} = \delta(\varepsilon - \varepsilon')\delta_{\nu\nu'} .$$

The state (2.2) is represented by the left-hand part (0) of the uppermost row: It couples via H to the states (a in Fig. 1)

$$|\varepsilon\rangle = \frac{1}{\sqrt{N_f}} \sum_\nu \psi^\dagger_\nu \psi_{\varepsilon\nu} |0\rangle , \tag{2.3}$$

in which one conduction electron below ε_F has hopped into the f level. The states $|\varepsilon\rangle$ couple to

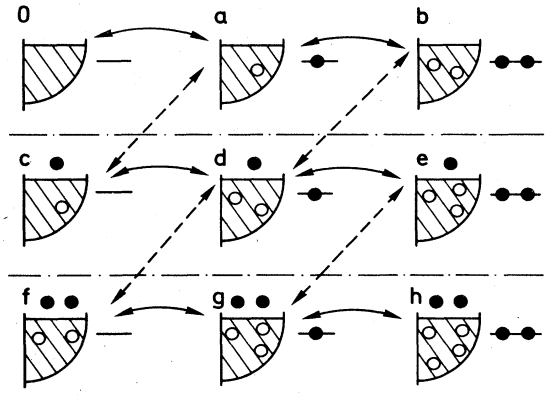

FIG. 1. Schematic representation of the basis states used. Solid circles show electrons; open circles, holes. In each part of the figure the conduction states are to the left and the f level to the right. The arrows show which states couple to each other and the strength of the coupling. A solid line indicates a strength $\sim \tilde{V}$ and a dashed line a strength $\tilde{V}/\sqrt{N_f}$.

$$|\varepsilon\varepsilon'\rangle = \frac{1}{\sqrt{N_f(N_f-1)}} \sum_{\substack{\nu,\nu' \\ \nu \neq \nu'}} \psi^\dagger_\nu \psi_{\varepsilon\nu} \psi^\dagger_{\nu'} \psi_{\varepsilon'\nu'} |0\rangle \tag{2.4}$$

and

$$|E\varepsilon\rangle = \frac{1}{\sqrt{N_f}} \sum_\nu \psi^\dagger_{E\nu} \psi_{\varepsilon\nu} |0\rangle . \tag{2.5}$$

For the states $|\varepsilon\varepsilon'\rangle$ (b in Fig. 1) another conduction electron has hopped into the f level, and the states $|E\varepsilon\rangle$ (c in the figure) describe how the f electron in $|\varepsilon\rangle$ can hop into an unoccupied conduction state with the energy E ($> \varepsilon_F$). The remaining states in Fig. 1 are constructed in a similar way. States with *more than two* f electrons are assumed to have such a high energy that they can be neglected. Alternatively, we could introduce an infinite three-body interaction. The neglect of states with more than two f electrons is, then, not an approximation. The states $|0\rangle$ and $|\varepsilon\rangle$ above were introduced by Varma and Yafet[14] in a variational calculation. To perform a ground-state calculation, the matrix elements of the Hamiltonian between the basis states are needed. In paper I we obtained

$$\langle \varepsilon | H | 0 \rangle = \tilde{V}(\varepsilon) , \tag{2.6}$$

$$\langle \varepsilon\varepsilon' | H | \varepsilon'' \rangle = \left[\frac{N_f - 1}{N_f} \right] [\, \tilde{V}(\varepsilon')\delta(\varepsilon - \varepsilon'') + \tilde{V}(\varepsilon)\delta(\varepsilon' - \varepsilon'')] , \tag{2.7}$$

$$\langle E\varepsilon | H | \varepsilon' \rangle = \frac{\tilde{V}(E)}{\sqrt{N_f}} \delta(\varepsilon - \varepsilon') , \tag{2.8}$$

where $\tilde{V}(\varepsilon)$ was defined Eq. (2.1). For a large N_f, the states in the first row of Fig. 1 couple with a strength which is independent of N_f, while the coupling between the states in the first and second rows varies as $1/\sqrt{N_f}$.

Since states with more than two f electrons are neglected, the states in the first row are the only ones which couple (indirectly) to $|0\rangle$ with a finite strength as $N_f \to \infty$. Similarly, the second and third rows contain all the states which couple with a strength $\sim 1/\sqrt{N_f}$ to the states in the row above. In the actual calculations, the states h are neglected for numerical convenience. For a finite (but possibly very large) system, the states in the first, second, and third rows give contributions to the total energy, $E_0(N)$, of the order of N_f^0, N_f^{-1}, and N_f^{-2}, respectively, in the limit of a large N_f. This shows how $1/N_f$ can be treated as a small parameter, and we will refer to this approach as the $1/N_f$ method. The analysis also justifies our choice (2.1) for $\tilde{V}(\varepsilon)$, since an N_f dependence of this type is needed to obtain a well-defined limit as $N_f \to \infty$. The ground-state properties are calculated variationally. In paper I we performed calculations by "folding" the Hamiltonian matrix, which is a very efficient method if not too many of the sets in Fig. 1 are included in the basis. If the matrix is written in a block form, the blocks in the diagonal are diagonal, and it is initially trivial to use the folding technique. In most cases, however, the folding produces nondiagonal elements in the remaining blocks and further folding of the matrix quickly becomes impractical. This technique is therefore simple only if the basis contains at most the states 0, a, b, and c or (for $U=\infty$) the states 0, a, c, and d. For a larger basis set the method presented below is more efficient.

The ground state is written as

$$|\phi\rangle = \sum_i c_i |i\rangle \ , \tag{2.9}$$

where $|i\rangle$ are (some of) the basis states in Fig. 1. We must then solve the eigenvalue problem

$$\sum_j H_{ij} c_j = E_0(N) c_i \ , \tag{2.10}$$

where the H_{ij} are the matrix elements of H, and $E_0(N)$ is the ground-state energy. The energy scale is transformed[15] linearly, so that the eigenvalues of the transformed matrix $\tilde{H}$ lie in the interval $[a,b]$, where $a<-1$ and $b\leq 1$. We guess an approximate ground-state V_0 of $\tilde{H}$, which can be written as

$$V_0 = \sum_\nu a_\nu v_\nu \ , \tag{2.11}$$

where the v_ν are the eigenvectors of $\tilde{H}$. The quantity

$$V_n \equiv T_n(\tilde{H}) V_0 = \sum_\nu a_\nu T_n(\varepsilon_\nu) v_\nu \tag{2.12}$$

is calculated,[15] where T_n is a Chebyshev polynomial of the order n, and ε_ν is an eigenvalue of $\tilde{H}$. For large values of n and $0<|x|-1\ll 1$,

$$T_n(x) \sim \tfrac{1}{2}\exp[n\sqrt{2(|x|-1)}] \ , \tag{2.13}$$

and (2.12) therefore approaches exponentially the eigenvector corresponding to the eigenvalue with the largest absolute value.[16] Because of the transformation of the energy scale, (2.12) gives the ground state. Owing to rounding errors, this is, in general, true, even if V_0 is orthogonal to the lowest eigenvector of $\tilde{H}$. The calculation of (2.12) is greatly simplified by the recursion formulas for the Chebyshev polynomials,

$$V_1 = \tilde{H} V_0 \ , \tag{2.14}$$

$$V_n = 2\tilde{H} V_{n-1} - V_{n-2}, \quad n \geq 2 \ . \tag{2.15}$$

To obtain a matrix $\tilde{H}$ of a finite size the energy variable is discretized into a finite number of points. The size of the matrix is essentially determined by the set of basis states with the largest number of continuum variables (E or ε). In this set, each state only couples to a few other basis states, and the matrix is very sparse.

The calculation of (2.14) and (2.15) is therefore relatively fast and the effort is essentially proportional[17] to N, if the matrix $\tilde{H}$ has the size $N\times N$. This is in contrast to a diagonalization of $\tilde{H}$, for which the work is proportional to N^3. The present method, in addition, makes the storage of an $N\times N$ matrix unnecessary, which for the basis sets discussed here would be quite unfeasible.

III. RESULTS FOR THE NONDEGENERATE AND SPIN-DEGENERATE CASES

The basis set in Fig. 1 is intended for a large degeneracy, N_f, and its suitability for a small N_f is less clear. For instance, it does not automatically lead to equal f^0 and f^2

TABLE I. The energy lowering, $\Delta E-\varepsilon_f$, for different values of the f-level energy ε_f, in the nondegenerate ($N_f=1$) Anderson model. The notations for the basis set refer to Fig. 1. The results (Ref. 18) on a given row were obtained using the set indicated in the leftmost column together with the ones in the rows above. For instance, the results in the third row were obtained with the basis sets a, c, and d. The states b and e do not enter for $N_f=1$, since they describe double occupancy. The parameters are $V=1.5$ and $B=6$ ($\tilde{\Delta}=0.75$), and the energy unit is eV.

Basis set	$\Delta E-\varepsilon_f$				
	$\varepsilon_f=2$	$\varepsilon_f=0$	$\varepsilon_f=-1$	$\varepsilon_f=-2$	$\varepsilon_f=-4$
a	−0.263	−0.534	−0.054	−0.001	−0.000
c	−0.290	−0.679	−0.359	−0.264	−0.177
d	−0.293	−0.714	−0.408	−0.291	−0.188
f	−0.293	−0.723	−0.415	−0.294	−0.189
g	−0.294	−0.726	−0.416	−0.294	−0.189
Exact	−0.294	−0.726	−0.416	−0.294	−0.189

TABLE II. The f occupancy (Ref. 18), n_f, for different values of ε_f in the nondegenerate ($N_f=1$) Anderson model. The parameters are $V=1.5$ and $B=6$ ($\tilde{\Delta}=0.75$). For the basis-set notation, see Fig. 1 and Table I. All energies are in eV.

Basis set	n_f $\varepsilon_f=2$	$\varepsilon_f=0$	$\varepsilon_f=-1$	$\varepsilon_f=-2$	$\varepsilon_f=-4$
a	0.065	0.283	0.813	0.996	1.000
c	0.081	0.444	0.853	0.934	0.971
d	0.083	0.487	0.833	0.919	0.967
f	0.083	0.499	0.824	0.916	0.967
g	0.084	0.497	0.822	0.916	0.967
Exact	0.084	0.500	0.822	0.916	0.967

weights for the symmetric Anderson model. The $N_f=1$ and the (symmetric) $N_f=2$ models are, however, good test cases, since the method should be least accurate for small values of N_f and since these two cases are best known from other calculations. The accuracy of the $1/N_f$ expansion in a slightly different formulation has been discussed thoroughly for $U=\infty$ by Rasul and Hewson,[12] who concentrated on properties other than those discussed below.

We first study the $N_f=1$ model, which is a one-body problem and therefore can be solved exactly. The exact solution is compared with results obtained using different basis sets. In Table I we show results for $\Delta E-\varepsilon_f$, where

$$\Delta E \equiv E_0(N)-\langle 0 \mid H \mid 0\rangle \ , \tag{3.1}$$

and $E_0(N)$ is the ground-state energy. When the hopping matrix elements $V(\varepsilon)$ are turned on, the energy is lowered by $\Delta E-\varepsilon_f$ relative to a state with one f electron and no hopping. The results for the f occupancy, n_f, are given in Table II. These results are obtained using a semielliptical form for $[V(\varepsilon)]^2$,

$$[V(\varepsilon)]^2=F(\varepsilon)\equiv 2V^2(B^2-\varepsilon^2)^{1/2}/(\pi B^2), \quad |\varepsilon| \le B \tag{3.2}$$

where $2B$ is the bandwidth, and the band is assumed to be symmetric around $\varepsilon_F=0$. We also define

$$\tilde{\Delta}\equiv N_f\Delta\equiv N_f\pi V^2(\varepsilon_F)=2N_fV^2/B \tag{3.3}$$

as a simple measure for the strength of the coupling between the f level and the conduction band.

For $N_f=1$ the basis set $\{\,|0\rangle, |\varepsilon\rangle\}$ [Eqs. (2.2) and (2.3)], referred to as a in Tables I and II, leads to rather inaccurate results, and for $-\varepsilon_f \gg \tilde{\Delta}=0.75$, it fails dramatically. However, basis set c, which also includes $\{\,|E\varepsilon\rangle\}$ [Eq. (2.5)], already gives much more accurate results. As the size of the basis set is increased, the results rapidly approach the exact results. For basis set g the errors in ΔE and n_f due to the limited basis set are usually smaller than the numerical accuracy of the calculation.

It is also interesting to study the spin-degenerate ($N_f=2$) model, where the states describing double occupancy enter. Although we generally expect the accuracy of the $1/N_f$ method to increase with N_f, the accuracy is not necessarily better for $N_f=2$ than for $N_f=1$. The reason is that, for $N_f=2$, new basis states enter, since states with two conduction holes can have these holes in different channels ν for $N_f \ge 2$. We focus on the symmetric case, $2\varepsilon_f+U=0$, for which the exact f^0 and f^2 weights are equal. The convergence with the size of the basis set is illustrated in Table III. Also for $N_f=2$, the basis set corresponding to the first row in Fig. 1 (first row in Table III) is not very good. For small values of V, the f^0 weight is much smaller than the f^2 weight, and for large values of V the opposite is true. As the size of the basis set is increased, the total energy is lowered and the f^0 and f^2 weights approach each other, as they should. The results are compared with the results from a quite different method, which is particularly suited for the $N_f=2$ case. This is also a variational method, where the basis states are obtained by projecting out appropriate

TABLE III. The energy $\Delta E-\varepsilon_f$ and the f^0, f^1, and f^2 weights (Ref. 18) for the symmetric ($N_f=2$) Anderson model. The parameters are $\varepsilon_f=-2.5$, $U=5$, and $B=6$, and two values of V are considered. For the basis-set notation, see Table I. The lowest row (Proj.) shows results of a projection-operator method described in Appendix A. All energies are in eV.

Basis set	$V=1$, $\tilde{\Delta}=0.67$ $\Delta E-\varepsilon_f$	f^0	f^1	f^2	$V=2$, $\tilde{\Delta}=2.67$ $\Delta E-\varepsilon_f$	f^0	f^1	f^2
$0+a+b$	−0.108	0.001	0.974	0.025	−0.628	0.141	0.778	0.081
c	−0.210	0.024	0.953	0.024	−0.899	0.150	0.779	0.072
$d+e$	−0.238	0.031	0.938	0.031	−1.126	0.140	0.745	0.115
f	−0.243	0.033	0.934	0.033	−1.185	0.138	0.736	0.126
g	−0.245	0.034	0.931	0.034	−1.217	0.137	0.732	0.132
Proj.	−0.214	0.033	0.933	0.033	−1.226	0.140	0.719	0.140

TABLE IV. The energy $\Delta E-\varepsilon_f$ and the f^0, f^1, and f^2 weights (Ref. 18) in the symmetric Anderson model according to the $1/N_f$ and projection-operator methods. The parameters are $\varepsilon_f=-2.5$, $U=5$, and $B=6$, and the energy unit is eV.

	$\Delta E-\varepsilon_f$		f^0		f^1		f^2	
V	$1/N_f$	Proj.	$1/N_f$	Proj.	$1/N_f$	Proj.	$1/N_f$	Proj.
1.0	−0.245	−0.214	0.034	0.033	0.931	0.933	0.034	0.033
1.5	−0.639	−0.618	0.088	0.096	0.825	0.808	0.087	0.096
2.0	−1.217	−1.226	0.137	0.140	0.732	0.719	0.132	0.140
3.0	−2.692	−2.737	0.186	0.184	0.637	0.632	0.177	0.184

parts of the Hartree-Fock solution of a related model problem. By construction this method gives the same f^0 and f^2 weights for the symmetric Anderson model. The method is described in detail in Appendix A. In Table IV we compare the results for $\Delta E-\varepsilon_f$ and the f^0, f^1, and f^2 weights obtained in the $1/N_f$ and projection-operator methods. The projection-operator method is particularly well suited for large values of V, where a Hartree-Fock solution is a good starting point. For $V=2$ and 3 this method gives a slightly lower total energy, while the $1/N_f$ method gives a somewhat better total energy for $V=1$ and 1.5. In all cases, however, both methods give similar results.

The accuracy of the $1/N_f$ method may seem surprising in view of the orthogonality catastrophe.[19] This theorem states that if a local perturbation is introduced in a system of electrons, the overlap between the unperturbed and perturbed ground states varies as $CN^{-\alpha}$, where N is the number of atoms of the system and α is related to the phase shifts of the perturbation. For the present problem the theorem implies that the overlap between the approximate and exact ground states goes to zero as $N\to\infty$. This has led to doubts[13] about the present approach, and below we therefore discuss in detail why in the limit $N_f\to\infty$ exact results are obtained for the physical properties studied.

We first considered a linear chain with N atoms. Each atom has a nondegenerate level at the energy zero and a hopping matrix element t to the nearest neighbors. This represents the unperturbed problem. The perturbed system has an additional atom with a nondegenerate level at ε_f and a hopping matrix element V to the last atom of the unperturbed chain. The unperturbed and perturbed systems both have N electrons. In the limit $N\to\infty$ this model goes over to the model described by Eq. (3.2). In Table V results are shown for the occupancy n_f of the additional atom and for $\Delta E-\varepsilon_f+\varepsilon_F^0$, where ε_F^0 is defined as the energy of the highest occupied orbital in the unperturbed system. The quantity $\Delta E-\varepsilon_f+\varepsilon_F^0$ corresponds to the energy lowering due to hopping, which was studied in the preceding tables. The table also shows the weight $\sum_i |\langle i|\phi\rangle|^2$ of the ground state $|\phi\rangle$ in some of the spaces $\{|i\rangle\}$ defined by Fig. 1. Table V shows the rapid convergence of the "local" properties $\Delta E-\varepsilon_f+\varepsilon_F^0$ and n_f with N. Both quantities converge as $1/N$, and for $N=200$ they only differ by a few percent from the $N=\infty$ results. Simultaneously, the reduction of the overlap between the exact ground state and the larger basis sets is rather small. Even for $N=200$ the exact ground state has only 0.2% of its weight outside the space defined by the two uppermost rows in Fig. 1. Thus the basis set in Fig. 1 can describe rather accurately the change of the wave function as N is increased up to some quite large value. If N is further increased, a larger basis set is required to describe the changes in the *wave function.* However, "local" properties, such as n_f and $\Delta E-\varepsilon_f+\varepsilon_F^0$, change little as N is increased from a large value to infinity. The basis set of Fig. 1 can therefore describe these properties well even for an infinite system. This is confirmed by comparing Table V with Tables I and II.

We now generalize the linear chain and introduce a degeneracy N_f and a Coulomb interaction U between two

TABLE V. The energy $\Delta E-\varepsilon_f+\varepsilon_F^0$, the f occupancy n_f, and the weight of the exact ground state, $|\phi\rangle$, in various subspaces for a linear chain with $N+1$ atoms. The columns 0, a, c, and d show the weight of $|\phi\rangle$ in the spaces defined by the states 0, $0+a$, $0+a+c$, and $0+a+c+d$, respectively, in Fig. 1. The parameters are $t=3$, $V=1.5$, and $\varepsilon_f=-1$. All energies are in eV.

N	$\Delta E-\varepsilon_f+\varepsilon_F^0$	n_f	0	a	c	d
10	−0.838	0.566	0.385	0.950	0.999	0.999 997
18	−0.635	0.676	0.244	0.920	0.997	0.999 98
26	−0.563	0.725	0.183	0.901	0.994	0.999 94
38	−0.514	0.757	0.136	0.883	0.990	0.999 9
50	−0.489	0.774	0.110	0.871	0.987	0.999 8
70	−0.468	0.788	0.086	0.856	0.982	0.999 6
100	−0.452	0.799	0.066	0.842	0.976	0.999 3
150	−0.440	0.807	0.050	0.826	0.968	0.999
200	−0.434	0.811	0.041	0.815	0.962	0.998
∞	−0.416	0.822				

TABLE VI. The energy $\Delta E-\varepsilon_f$, the f occupancy n_f, and the weight of the various basis sets for the ground state of a finite system with $N+1=31$ atoms. The basis set notation $(0,a,\ldots)$ refers to Fig. 1. For $N_f=1$ the $1/N_f$ results are compared with an exact calculation, and for $N_f=6$ and 14 the $1/N_f$ results for $U=\infty$ and 5 are compared. The parameters are $t=3$, $\tilde{V}=\sqrt{N_f}V=1.5$, and $\varepsilon_f=-1$. The energy unit is eV.

	$N_f=1$	$N_f=6$		$N_f=14$	
		$U=\infty$	$U=5$	$U=\infty$	$U=5$
$\Delta E-\varepsilon_f$, $1/N_f$,	−0.237 872 062	−0.0260	−0.1178	−0.0001	−0.1637
$\Delta E-\varepsilon_f$, Exact,	−0.237 872 067				
n_f, $1/N_f$,	0.738 693 355	0.6952	0.7331	0.6860	0.7856
n_f, Exact,	0.738 693 352				
0	0.162 9	0.2829	0.2181	0.3043	0.2309
a	0.7315	0.6910	0.7228	0.6840	0.7266
b			0.0251		0.0269
c	0.098 3	0.0219	0.0232	0.0097	0.0104
d	0.007 2	0.0042	0.0103	0.0020	0.0049
e			0.0003		0.0002
f	0.89×10^{-4}	0.69×10^{-4}	0.19×10^{-3}	0.15×10^{-4}	0.40×10^{-4}
g	0.44×10^{-6}	0.56×10^{-5}	0.32×10^{-4}	0.14×10^{-5}	0.78×10^{-5}

electrons in the ε_f level. The chain has N_f N electrons. Results are shown in Table VI for $N=30$ in the cases $N_f=1$, 6, and 14. The results for $N_f=1$ are compared with the exact results. This comparison is a good test of both our formal calculations and the computer program. Comparison of the results for $N_f=6$ and 14 shows that for given values of N and $\tilde{V}=\sqrt{N_f}V$, the basis functions of the second and third rows play a much smaller role as N_f is increased.[20] This was expected since the coupling between the states in two adiacent rows varies as $\tilde{V}/\sqrt{N_f}$. As N_f is increased, the infrared catastrophe therefore shows up for increasingly large values of N,[21] and "local" properties, such as n_f, are increasingly accurately described even for an infinite system. For $N_f=\infty$ these properties are given exactly. This is illustrated in Fig. 2, where we compare the results obtained for the charge and spin susceptibility for $U=\infty$, using the exact Bethe ansatz[3] and the smallest nontrivial basis set in the $1/N_f$ method. The figure also compares the $1/N_f$ results[10] for the value of the valence photoemission spectrum at ε_F with the exact results from Friedel's sum rule.[22] The results obtained in the $1/N_f$ scheme approach the exact results for $N_f\to\infty$, as they should, while some alternative approaches[13] do not satisfy Friedel's sum rule.[23] To further illustrate the convergence with N_f, we show in Table VII some results for an infinite system with $N_f=14$. We have chosen $V=0.8\approx2/\sqrt{7}$, and the table should be compared with the results for $V=2$ and $N_f=2$ in Table III. The larger f^2 weight in Table VII for the basis set $0+a+b$ is due to the $\sqrt{(N_f-1)/N_f}$ dependence of the matrix element $\langle\varepsilon\varepsilon'|H|\varepsilon''\rangle$ in Eq. (2.7). While the f^0-to-f^1 coupling is similar, the f^1-to-f^2 coupling is therefore effectively stronger for $N_f=14$ and the basis set $0+a+b$.

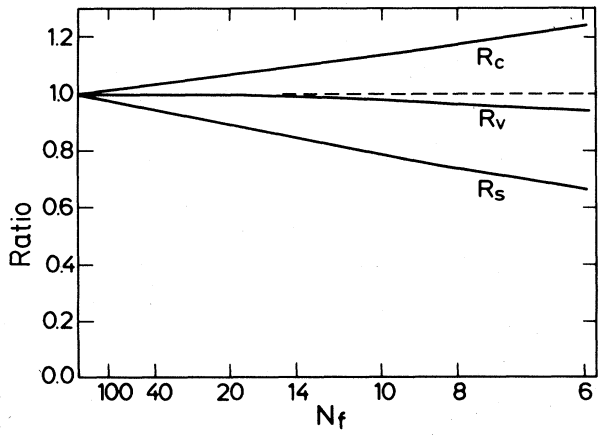

FIG. 2. Results for the charge (R_c) and spin (R_s) susceptibility as well as the spectral weight (R_v) at the Fermi energy. The figure shows the ratio between the results using the smallest nontrivial basis set in the $1/N_f$ method and the exact results (Refs. 3 and 22).

Comparison of the smallest and largest basis sets shows the difference in convergence for $N_f=2$ and 14. For $N_f=2$, $\Delta E-\varepsilon_F$ changes by a factor of 2 and f^2 changes by 0.05, while for $N_f=14$ these changes are 11% and 0.01, respectively.

IV. LARGE DEGENERACY

In the Introduction it was pointed out that even for "symmetric" parameters, $2\varepsilon_f+U=0$, the f^0 and f^2 states can play a very different role for $N_f>2$. This is illustrated in Table VIII, which shows the weights of the f^0, f^1, and f^2 states as a function of V. For large values of V the f^0 and f^2 weights are not very different. For small values of V, however, the f^2 weight is much larger than the f^0 weight, and for $V=0.3$ the difference is a factor of 10.

In order to understand the asymmetry between the f^0 and f^2 states for a sufficiently large N_f, we discuss in this section the limit of infinite degeneracy ($N_f\to\infty, N_f\Delta=\tilde{\Delta}=$const). For an arbitrary large but finite system the first row of basis states in Fig. 1 then

TABLE VII. The energy $\Delta E-\varepsilon_f$ and the f^0, f^1, and f^2 weights (Ref. 18) for $N_f=14$. The parameters are $\varepsilon_f=-2.5$, $U=5$, $B=6$, and $V=0.8$ ($\tilde{\Delta}=2.99$). For the basis-set notation, see Table I. All energies are in eV.

Basis set	$\Delta E-\varepsilon_f$	f^0	f^1	f^2
$0+a+b$	−1.094	0.128	0.738	0.134
c	−1.132	0.130	0.738	0.132
$d+e$	−1.202	0.128	0.730	0.142
f	−1.206	0.128	0.730	0.142
g	−1.211	0.128	0.730	0.143

leads to the exact ground state. In addition to the ground state, we discuss "magnetic" states of the system. The main points of this section are (i) the definition of a "Kondo temperature," δ_u [Eq. (4.12)], (ii) results for δ_u [Eqs. (4.15) and (4.16), and Table IX], (iii) results for the f^0, f^1, and f^2 weights in terms of δ_u [Eq. (4.17) and the following discussion], and (iv) an equation for the spin susceptibility [Eq. (4.18)]. The ground state in the limit of infinite degeneracy is of the form

$$|\phi_0\rangle=A\left[\,|0\rangle+\int_{-B}^{0}a(\varepsilon)\,|\varepsilon\rangle+\int_{-B}^{0}d\varepsilon\int_{-B}^{\varepsilon}d\varepsilon'\,b(\varepsilon,\varepsilon')\,|\varepsilon,\varepsilon'\rangle\,\right], \tag{4.1}$$

where the basis states $|\varepsilon\rangle$ and $|\varepsilon,\varepsilon'\rangle$ are defined in (2.3) and (2.4). With the matrix elements (2.6) and (2.7) and the definition (3.1), the Schrödinger equation for the ground state reads

$$\Delta E=\int_{-B}^{0}\tilde{V}(\varepsilon)a(\varepsilon)d\varepsilon\,, \tag{4.2}$$

$$[\varepsilon_f-\varepsilon-\Delta E-(N_f-1)\tilde{\Gamma}(2\varepsilon_f+U-\varepsilon-\Delta E)]a(\varepsilon)+\tilde{V}(\varepsilon)\left[1-\left[1-\frac{1}{N_f}\right]\int_{-B}^{0}\frac{\tilde{V}(\varepsilon_1)a(\varepsilon_1)}{2\varepsilon_f+U-\varepsilon-\Delta E-\varepsilon_1}d\varepsilon_1\right]=0\,, \tag{4.3}$$

where

$$\tilde{\Gamma}(z)=\int_{-B}^{0}\frac{[V(\varepsilon)]^2}{z-\varepsilon}d\varepsilon \tag{4.4}$$

and the coefficients

$$b(\varepsilon,\varepsilon')=-\frac{\sqrt{N_f-1}}{2\varepsilon_f+U-\Delta E-\varepsilon-\varepsilon'}[V(\varepsilon)a(\varepsilon')+V(\varepsilon')a(\varepsilon)] \tag{4.5}$$

describing the double occupancy have been eliminated using $\langle\varepsilon\varepsilon'\,|\,(H-E_0)\,|\,\phi_0\rangle=0$.

In these equations we have not yet replaced expressions like N_f-1 by N_f because the above equations also describe the exact ground state for finite N_f if the valence band is completely filled.

In contrast to the limit $U\to\infty$, Eq. (4.3) is an integral equation for $a(\varepsilon)$, which only in the limit $B\ll U$ is of a separable form. In this limit we have

$$\int_{-B}^{0}\frac{\tilde{V}(\varepsilon_1)a(\varepsilon_1)}{2\varepsilon_f+U-\Delta E-\varepsilon-\varepsilon_1}d\varepsilon_1\approx\frac{1}{2\varepsilon_f+U-\Delta E}\int_{-B}^{0}\tilde{V}(\varepsilon_1)a(\varepsilon_1)d\varepsilon_1=\frac{\Delta E}{2\varepsilon_f+U-\Delta E}\,. \tag{4.6}$$

Inserting (4.3) into (4.2) and using (4.6), we obtain the transcendental equation for ΔE,

TABLE VIII. The energy $\Delta E-\varepsilon_f$, the f^0, f^1, and f^2 weights, and the susceptibility (Ref. 18) for the Anderson model with the degeneracy $N_f=14$. The parameters are $\varepsilon_f=-2.5$, $U=5$, and $B=6$. The susceptibility is calculated for $j=\frac{13}{2}$ and the results are given in units of $(g\mu_B)^2$. All energies are in eV.

V	$\Delta E-\varepsilon_f$	f^0	f^1	f^2	χ
0.3	−0.138	0.003	0.967	0.030	
0.4	−0.249	0.011	0.937	0.052	4×10^3
0.5	−0.407	0.035	0.885	0.080	5.2×10^2
0.6	−0.626	0.070	0.824	0.107	1.66×10^2
0.8	−1.211	0.128	0.730	0.143	4.93×10^1
1.0	−1.918	0.162	0.672	0.166	2.64×10^1

$$\Delta E = -\left[1-\left[1-\frac{1}{N_f}\right]\frac{\Delta E}{2\varepsilon_f+U-\Delta E}\right]\int_{-B}^{0}\frac{N_f V^2(\varepsilon)}{\varepsilon_f-\Delta E-(N_f-1)\tilde{\Gamma}(2\varepsilon_f+U-\Delta E-\varepsilon)-\varepsilon}d\varepsilon$$

$$\approx -\left[1-\left[1-\frac{1}{N_f}\right]\frac{\Delta E}{2\varepsilon_f+U-\Delta E}\right]N_f\tilde{\Gamma}(\varepsilon_f-\Delta E-(N_f-1)\tilde{\Gamma}(2\varepsilon_f+U-\Delta E))\ . \tag{4.7}$$

In the second line we have again used $U \gg B$. Before we discuss this equation, it is useful to consider also "magnetic" eigenstates, i.e., those eigenstates that are not totally symmetric with respect to permutations of the ν label. Such states can be constructed starting from basis states

$$|\varepsilon, m_{(i)}\rangle = \sum_{\nu} C_{\nu}^{(i)} \psi_{\nu}^{\dagger}\psi_{\varepsilon\nu}|0\rangle\ , \tag{4.8}$$

with $\sum_{\nu}(C_{\nu}^{(i)})^2=1$ and $\sum_{\nu} C_{\nu}^{(i)}=0$. These states do *not* couple via H to $|0\rangle$, but couple to the $f^{(2)}$ states,

$$|\varepsilon,\varepsilon' m_{(i)}\rangle = \frac{1}{\sqrt{N_f-1}}\sum_{\substack{\nu,\nu'\\ \nu\neq\nu'}} \psi_{\nu}^{\dagger}\psi_{\varepsilon\nu}C_{\nu}^{(i)}\psi_{\nu'}^{\dagger}\psi_{\varepsilon'\nu'}|0\rangle\ , \tag{4.9}$$

with $-B<\varepsilon,\varepsilon'<0$, but no restriction on the sign of $\varepsilon-\varepsilon'$. In the limit $N_f\to\infty$ these states are orthonormalized and produce no indirect coupling between the $|\varepsilon, m_{(i)}\rangle$ with different energies ε. Then the energy lowering $\Delta E_{\varepsilon,m_{(i)}}$ due to the hybridization of the states (4.8) and (4.9) can easily be calculated for arbitrary U and is determined by

$$\Delta E_{\varepsilon,m_{(i)}} = -\bar{\Gamma}(\varepsilon_f+U-\Delta E_{\varepsilon,m_{(i)}})\ , \tag{4.10}$$

with

$$\bar{\Gamma}(z) = \int_{-B}^{0}\frac{\tilde{V}^2(\varepsilon)}{z-\varepsilon}d\varepsilon\ .$$

$\Delta E_{\rm mag}\equiv\Delta E_{\varepsilon,m_{(i)}}$ is independent of ε and of the special choice of $C_{\nu}^{(i)}$. The f^2 occupancy of the magnetic states is given by

$$\langle P_2\rangle_{\rm mag} = \frac{-\bar{\Gamma}'(\varepsilon_f+U-\Delta E_{\rm mag})}{1-\bar{\Gamma}'(\varepsilon_f+U-\Delta E_{\rm mag})}\ , \tag{4.11}$$

where $\bar{\Gamma}'(\varepsilon)=d\bar{\Gamma}(\varepsilon)/d\varepsilon$. The f^0 occupancy of the magnetic states vanishes identically, and for $\langle P_2\rangle_{\rm mag}\ll 1$ the f^2 occupancy varies quadratically with V. The lowest-energy magnetic state of this type is obtained by setting $\varepsilon\approx\varepsilon_F$ in (4.8), which leads to an energy $\langle 0|H|0\rangle+\varepsilon_f+\Delta E_{\rm mag}$.

Magnetic states with a lower energy can be obtained by starting with

$$|0m_{(i)}\rangle = \sum_{\nu} C_{\nu}^{(i)}\psi_{E\nu}^{\dagger}\psi_{\varepsilon\nu}|0\rangle\ .$$

From this state we can generate states with one and two f electrons and form linear combinations. If E and ε are sufficiently close to zero, we obtain "magnetic" states with a lower energy than in the approach above. These states do not, however, couple to the $N_f\to\infty$ ground state via operators of interest here [e.g., S_Z in Eq. (B1)]. We therefore focus on the magnetic states defined above.

The important energy for the low-temperature thermodynamic properties and for the behavior of the valence spectrum near the Fermi energy is the *energy difference δ_u between the nonmagnetic ground state and the lowest magnetic states* in the space (4.8) and (4.9). We therefore introduce this energy difference, which is related to the Kondo temperature, by

$$\Delta E\equiv E_0-\langle 0|H|0\rangle\equiv\varepsilon_f+\Delta E_{\rm mag}-\delta_u\ . \tag{4.12}$$

δ_u is important for the valence spectrum near $\varepsilon_F=0$ since the variation of $a(\varepsilon)$ for energies $-\delta_u\le\varepsilon<0$ is essentially determined by δ_u. Assuming that $\varepsilon_+\equiv\varepsilon_f+U-\Delta E_{\rm mag}\gg\delta_u$, we can perform a Taylor expansion in Eq. (4.3) and obtain, near ε_F,

$$a(\varepsilon)\approx\frac{\tilde{V}(\varepsilon)}{\varepsilon-\delta_u}\left[1-\int_{-B}^{0}\frac{\tilde{V}(\varepsilon_1)a(\varepsilon_1)}{\varepsilon_+-\varepsilon_1}d\varepsilon_1\right](1-\langle P_2\rangle_{\rm mag})\ . \tag{4.13}$$

As discussed below, in the spin-fluctuation limit, $-\varepsilon_f\gg\tilde{\Delta}$, the energy difference δ_u is exponentially small and $a(\varepsilon)$ shows the same sharp rise as in the limit $U\to\infty$.

For $U\gg B$ the behavior of δ_u as a function of U can be obtained from (4.7). We restrict our discussion to the spin-fluctuation limit. Then δ_u is much smaller than $|\varepsilon_f|$, ε_+, and $|\Delta E_{\rm mag}|$, and (4.7) simplifies in the limit $N_f\to\infty$ to

$$-\bar{\Gamma}(\delta_u)=\frac{\varepsilon_f+\Delta E_{\rm mag}}{1-(\varepsilon_f+\Delta E_{\rm mag})/\varepsilon_+}\equiv\varepsilon_0(u)\ . \tag{4.14}$$

For a constant band density of states [$\tilde{V}(\varepsilon)=$const] this leads to

$$\delta_u = B\exp\left[\frac{\varepsilon_0(U)}{\tilde{\Delta}/\pi}\right]\ . \tag{4.15}$$

To leading order in $1/U$ the hybridization energy $\Delta E_{\rm mag}$ follows from (4.10) as $-B(\tilde{\Delta}/\pi)/(\varepsilon_f+U)$. For $\varepsilon_0(U)$ one then obtains, to leading order in $1/U$,

$$\varepsilon_0(U)\approx\varepsilon_f-\frac{B\tilde{\Delta}/\pi-\varepsilon_f^2}{\varepsilon_f+U}\ . \tag{4.16}$$

In the limit $U\gg B$ the "Kondo temperature" δ_u therefore increases with decreasing U if $\varepsilon_f^2>B\tilde{\Delta}/\pi$ and decreases if $B\tilde{\Delta}/\pi>\varepsilon_f^2$. The behavior of δ_u therefore very explicitly depends on the bandwidth B. The behavior of δ_u as a function of U for an arbitrary ratio of U/B is obtained numerically and shown in Table IX.

The occupancy of the f level in the ground state is given by $n_f=\langle P_1\rangle+2\langle P_2\rangle$, where the weights $\langle P_1\rangle$ and $\langle P_2\rangle$ of the f^1 and f^2 contributions follow from (4.1) and (4.5) as

$$\langle P_1\rangle = A^2\int_{-B}^{0}[a(\varepsilon)]^2 d\varepsilon \equiv A^2 I_1 ,$$

$$\langle P_2\rangle = A^2\left[\int_{-B}^{0} d\varepsilon\, a(\varepsilon)\tilde{V}(\varepsilon)\int_{-B}^{0}\frac{a(\varepsilon')\tilde{V}(\varepsilon')d\varepsilon'}{(\varepsilon_+ +\delta_u-\varepsilon-\varepsilon')^2}+\int_{-B}^{0} d\varepsilon[\tilde{V}(\varepsilon)]^2\int_{-B}^{0}\frac{[a(\varepsilon')]^2}{(\varepsilon_+ +\delta_u-\varepsilon-\varepsilon')^2}d\varepsilon'\right]\equiv A^2 I_2 , \quad (4.17)$$

and $A^2=\langle P_0\rangle=(1+I_1+I_2)^{-1}$. In the spin-fluctuation limit, the integral I_1 is dominated by the contribution near the Fermi energy, where (4.13) can be used. This leads to a contribution proportional to $\tilde{\Delta}/\delta_u$. The value of I_2 in the spin-fluctuation limit is largely determined by the second integral in (4.17). As $[a(\varepsilon)]^2$ is strongly peaked at the Fermi energy, the denominator in the ε' integral can therefore be taken at $\varepsilon'=0$. This yields $I_2\approx I_1\tilde{\Gamma}'(\varepsilon_+)$. The f^0 weight A^2 is therefore "exponentially" small and the f^2 weight of the (nonmagnetic) ground state is approximately equal to $\langle P_2\rangle_{\rm mag}$, the f^2 weight of the magnetic states (4.11), which varies quadratically with V. This result shows the different role of the f^0 and f^2 states discussed in the introduction to this section. The f occupancy n_f is, in the spin-fluctuation limit, given by $n_f\approx 1+\langle P_2\rangle_{\rm mag}$. Here we have kept the notation "spin-fluctuation limit" for the case where the "Kondo temperature" δ_u is exponentially small, although $\langle P_2\rangle$ may not be very small and n_f is not necessarily very close to 1.

The dependence of the magnetic susceptibility on the f_0 and f_2 weights for large degeneracy N_f differs very much from the behavior for the spin-degenerate case $N_f=2$. For $N_f=2$ the susceptibility is small if either the f^0 or f^2 weight is large.[8] This may suggest that the f^2 weight mainly determines the susceptibility in the spin-fluctuation limit for $N_f\gg 2$ since $\langle P_2\rangle\gg\langle P_0\rangle$. That this conclusion is incorrect follows from the result $\langle P_2\rangle\approx\langle P_2\rangle_{\rm mag}$ discussed above: An *arbitrary* linear combination of states $\psi_\nu^\dagger\psi_{\varepsilon\nu}|0\rangle$ leads to approximately the same f^2 weight, i.e., the attempt to line up the spin in a certain direction by a magnetic field does not interfere with the energy gain due to the hybridization with the f^2 states. It is the additional energy lowering, δ_u, of the nonmagnetic ground state, arising from the coupling to the state $|0\rangle$, which determines the magnetic susceptibility. The smaller δ_u, the smaller the magnetic field has to be to line up the spin. One therefore expects the susceptibility to be inversely proportional to δ_u. The calculation of the susceptibility is described in Appendix B. In the spin-fluctuation limit, the result simplifies to

$$\chi_0\approx\tfrac{1}{3}j(j+1)g^2\mu_B^2(1/\delta_u) , \quad (4.18)$$

which has the same form as we obtained in paper I for $U\to\infty$. This result confirms the important role played by the "Kondo temperature" δ_u. Its importance for the valence spectrum near the Fermi energy is discussed in the next section.

The analytical results presented in this section were mainly for the spin-fluctuation limit, i.e., very small V. The results presented are then accurate only for N_f larger than "realistic" values. For the smallest value of V in Table VIII ($N_f=14$), the calculation using the basis set of Fig. 1 gives such a small weight for $|0\rangle$ that even for $N_f=14$ the states $|E\varepsilon\rangle$ dominate the f^0 weight.

TABLE IX. The "Kondo" temperature [Eq. (4.12)] as a function of U. We have used a constant density of states with $\tilde{\Delta}=0.75$ and $B=24$. All quantities are in eV.

	δ_u	
U	$\varepsilon_f=-1.5$	$\varepsilon_f=-2.5$
∞	0.038	0.000 68
100	0.034	0.000 71
50	0.032	0.000 75
20	0.027	0.000 98
10	0.025	0.001 7
5	0.026	0.005 2
3	0.031	0.016

V. VALENCE SPECTRUM

Valence photoemission has frequently been used to study Ce mixed-valence compounds, since the valence spectrum should, for instance, contains information about the f-level position. In paper I we presented exact results of the valence photoemission (PE) spectrum for $U=\infty$ in the limit of infinite degeneracy. A "folding" technique was used to obtain corrections for a finite N_f. This method is very convenient for the basis states considered earlier. However, when double occupancy of the f level is allowed, the calculation of the PE spectrum becomes tedious, and a simpler time-dependent formalism is presented below.

The usefulness of a time-dependent formulation was demonstrated by Nozières and de Dominicis[24] for core spectroscopies. For noninteracting valence electrons ($N_f=1$), such a formulation makes it possible to calculate the exact core spectra of a generalized Anderson model,[25] while the calculations, in general, are very difficult for interacting valence electrons. Below we combine the time-dependent treatment and the $1/N_f$ idea to calculate the valence spectrum for the Hamiltonian (1.1) which contains the f-f interaction. We have also performed calculations using a moment method[26] (Lanczos method) and have obtained identical results within numerical accuracy, as we should.

We describe the valence PE process by the operator

$$T=\tau\sum_\nu\int d\tilde{E}\,\psi_{\tilde{E}\nu}^\dagger\psi_\nu + \frac{1}{\sqrt{N_f}}\sum_\nu\int d\tilde{E}\int_{-B}^{B} d\varepsilon\,\tau(\varepsilon)\psi_{\tilde{E}\nu}^\dagger\psi_{\varepsilon\nu} , \quad (5.1)$$

where $\psi_{\tilde{E}\nu}^\dagger$ creates a high-lying continuum state not in-

cluded in the model (1.1). Equation (5.1) includes the emission of both the f electrons and the conduction electrons which couple to the f electron. The remaining conduction states (see discussion in paper I) do not interfere with the f emission and are therefore not considered here. The magnitude of the emission from these states can be estimated from a band calculation, and we expect it to be a large fraction of the total conduction emission. The prefactor $1/\sqrt{N_f}$ in the second term has been introduced to make the emission of conduction electrons independent of N_f. This gives us a well-defined limit $N_f \to \infty$, and is in the same spirit as Eq. (2.1). In the sudden approximation[27] one assumes that the final states are of the form

$$\psi^\dagger_{\tilde{E}\nu} | E_n(N-1)\rangle , \tag{5.2}$$

where $| E_n(N-1)\rangle$ is an eigenstate of H with $N-1$ electrons. This is correct if $\tilde{E}$ is so large that the interaction between the emitted electron and the rest of the system can be neglected. The current of emitted electrons is then given by

$$j(\tilde{E}) = \sum_n | \langle E_n(N-1) | \psi_{\tilde{E}\nu} T | \phi \rangle |^2 \times \delta(\tilde{E} - \omega - E_0(N) + E_n(N-1)) , \tag{5.3}$$

which can be written as

$$j(\tilde{E}) = \frac{1}{\pi} \mathrm{Im} \times \sum_\nu \left\langle \phi \left| T^\dagger \psi^\dagger_{\tilde{E}\nu} \frac{1}{\tilde{E} - \omega - E_0(N) + H - i0^+} \psi_{\tilde{E}\nu} T \right| \phi \right\rangle , \tag{5.4}$$

where ω is the photon energy and $E_0(N)$ is the ground-state energy. Thus we must calculate the Green's function

$$g^<(z) = \left\langle \phi^< \left| \frac{1}{z+H} \right| \phi^< \right\rangle , \tag{5.5}$$

where

$$| \phi^< \rangle = \psi_{\tilde{E}\nu} T | \phi \rangle = \left[\tau \psi_\nu + \frac{1}{\sqrt{N_f}} \int d\varepsilon \, \tau(\varepsilon) \psi_{\varepsilon\nu} \right] | \phi \rangle . \tag{5.6}$$

Equation (5.5) can be rewritten as

$$g^<(z) = i \int_0^\infty dt \, e^{-izt} \langle \psi(0) | \psi(t) \rangle , \tag{5.7}$$

where

$$| \psi(t) \rangle = e^{-iHt} | \phi^< \rangle \tag{5.8}$$

describes the time evolution of the system after the photoelectron has been emitted. This state satisfies the time-dependent Schrödinger equation,

$$i \frac{\partial}{\partial t} | \psi(t) \rangle = H | \psi(t) \rangle , \tag{5.9}$$

with the initial condition

$$| \psi(0) \rangle = | \phi^< \rangle . \tag{5.10}$$

We express $| \psi(t) \rangle$ in terms of some bases set $\{ | j \rangle \}$ as

$$| \psi(t) \rangle = \sum_j c_j(t) e^{-iH_{jj}t} | j \rangle , \tag{5.11}$$

which leads to the equation

$$i \frac{\partial}{\partial t} c_j(t) = e^{iH_{jj}t} \sum_{k \, (\neq j)} H_{jk} e^{-iH_{kk}t} c_k(t) . \tag{5.12}$$

In Eq. (5.11) we have introduced the factor $\exp(-iH_{jj}t)$ to reduce the time dependence of $c_j(t)$. In a Runge-Kutta type of method for solving a system of linear differential equations, one repeatedly calculates the right-hand side of Eq. (5.12). Owing to the structure of H_{jk}, such a calculation requires relatively little time, a feature which was also the key idea leading to the method in Sec. II. Once the $\{c_j(t)\}$ have been obtained, we calculate

$$\langle \psi(0) | \psi(t) \rangle = \sum_j c_j^*(0) c_j(t) e^{-iH_{jj}t} \tag{5.13}$$

and perform the Fourier transform in Eq. (5.7). In practice, we introduce a broadening corresponding to the instrumental resolution. Therefore, z in (5.7) has a negative imaginary part and the integral (5.7) can be cut off at finite t.

The valence spectrum above the Fermi energy, which is sampled experimentally by bremsstrahlung isochromat spectroscopy (BIS), is, in the sudden approximation, described by

$$g^>(z) = \left\langle \phi^> \left| \frac{1}{z-H} \right| \phi^> \right\rangle , \tag{5.14}$$

where

$$| \phi^> \rangle = T^\dagger \psi^\dagger_{\tilde{E}\nu} | \phi \rangle = \left[\tau \psi^\dagger_\nu + \frac{1}{\sqrt{N_f}} \int dE \, \tau(E) \psi^\dagger_{E\nu} \right] | \phi \rangle . \tag{5.15}$$

Equation (5.14) is calculated in a similar way as Eq. (5.5).

For the calculation of the valence photoemission spectrum we use the ground state discussed in Sec. IV,

$$| \phi \rangle = A \left[| 0 \rangle + \int_{-B}^0 d\varepsilon \, a(\varepsilon) | \varepsilon \rangle + \int_{-B}^0 d\varepsilon \int_{-B}^{\varepsilon} d\varepsilon' \, b(\varepsilon, \varepsilon') \right] | \varepsilon\varepsilon' \rangle . \tag{5.16}$$

In photoemission one electron is removed and the basis states used to describe $| \psi(t) \rangle$ therefore contain one fewer electron. We use the states

$$| \varepsilon\nu \rangle = \psi_{\varepsilon\nu} | 0 \rangle , \tag{5.17}$$

$$| \varepsilon'\varepsilon\nu 1 \rangle = \frac{1}{\sqrt{N_f - 1}} \sum_{\nu' \, (\neq \nu)} \psi^\dagger_{\nu'} \psi_{\varepsilon'\nu'} \psi_{\varepsilon\nu} | 0 \rangle , \tag{5.18}$$

$$|\varepsilon'\varepsilon\nu 2\rangle=\psi_\nu^\dagger\psi_{\varepsilon'\nu}\psi_{\varepsilon\nu}|0\rangle\ , \tag{5.19}$$

$$|\varepsilon'\varepsilon''\varepsilon\nu 1\rangle=\frac{1}{\sqrt{(N_f-1)(N_f-2)}}\sum_{\nu'\ (\neq\nu)}\sum_{\nu''\ (\neq\nu)}\psi_\nu^\dagger\psi_{\varepsilon'\nu'}\psi_{\nu''}^\dagger\psi_{\varepsilon''\nu''}\psi_{\varepsilon\nu}|0\rangle\ , \tag{5.20}$$

$$|\varepsilon'\varepsilon''\nu 2\rangle=\frac{1}{\sqrt{N_f-1}}\sum_{\nu'\ (\neq\nu)}\psi_\nu^\dagger\psi_{\varepsilon'\nu'}\psi_{\nu'}^\dagger\psi_{\varepsilon''\nu}\psi_{\varepsilon\nu}|0\rangle\ . \tag{5.21}$$

The restrictions $\varepsilon'\geq\varepsilon$, $\varepsilon'\geq\varepsilon''$, and $\varepsilon''\geq\varepsilon$ are introduced in Eqs. (5.19), (5.20), and (5.21), respectively, to avoid a linearly dependent basis set. The time-dependent wave function [Eq. (5.11)] is written as

$$|\psi(t)\rangle=\frac{A}{\sqrt{N_f}}\left[\int_{-B}^{0}d\varepsilon\,a(\varepsilon,t)|\varepsilon\nu\rangle+\int_{-B}^{0}d\varepsilon'\int_{-B}^{0}d\varepsilon\,b_1(\varepsilon',\varepsilon,t)|\varepsilon'\varepsilon\nu 1\rangle+\int_{-B}^{0}d\varepsilon'\int_{-B}^{\varepsilon'}d\varepsilon\,b_2(\varepsilon',\varepsilon,t)|\varepsilon'\varepsilon\nu 2\rangle\right.$$
$$\left.+\int_{-B}^{0}d\varepsilon'\int_{-B}^{\varepsilon'}d\varepsilon''\int_{-B}^{0}d\varepsilon[c_1(\varepsilon',\varepsilon'',\varepsilon,t)|\varepsilon'\varepsilon''\varepsilon\nu 1\rangle+c_2(\varepsilon,\varepsilon',\varepsilon'',t)|\varepsilon\varepsilon'\varepsilon''\nu 2\rangle]\right]\ , \tag{5.22}$$

with the initial conditions

$$a(\varepsilon,0)=\tau(\varepsilon)+\tau a(\varepsilon)\ , \tag{5.23}$$

$$b_1(\varepsilon',\varepsilon,0)=\left[\frac{N_f-1}{N_f}\right]^{1/2}\tau(\varepsilon)a(\varepsilon')+\tau b(\varepsilon,\varepsilon')\ , \tag{5.24}$$

$$b_2(\varepsilon',\varepsilon,0)=\frac{1}{\sqrt{N_f}}[\tau(\varepsilon)a(\varepsilon')-\tau(\varepsilon')a(\varepsilon)]\ , \tag{5.25}$$

$$c_1(\varepsilon',\varepsilon'',\varepsilon,0)=\left[\frac{N_f-2}{N_f}\right]^{1/2}\tau(\varepsilon)b(\varepsilon',\varepsilon'')\ , \tag{5.26}$$

$$c_2(\varepsilon',\varepsilon'',\varepsilon,0)=\frac{1}{\sqrt{N_f}}[\tau(\varepsilon)b(\varepsilon',\varepsilon'')-\tau(\varepsilon'')b(\varepsilon',\varepsilon)]\ , \tag{5.27}$$

where we have defined

$$b(\varepsilon',\varepsilon)=b(\varepsilon,\varepsilon')\ \text{ for }\varepsilon>\varepsilon'\ . \tag{5.28}$$

For $N_f=\infty$ this approach gives the exact spectrum if more than double occupancy can be neglected. If $\tau(\varepsilon)\equiv 0$, the integrated weights of the valence and BIS spectra are proportional to n_f and N_f-n_f, respectively. To obtain a comparable accuracy for the BIS and PE spectra, we therefore use one more row of basis states in the BIS calculation. Thus, the first two rows of Fig. 1 are used for the ground-state calculation. To describe $|\psi(t)\rangle$ we use states which are the same as the states a—e in Fig. 1, except that all the states have one fewer conduction hole.

For the valence PE spectrum it is useful to introduce the states ($N_f\rightarrow\infty$)

$$|\tilde{\varepsilon}\nu\rangle=\psi_{\varepsilon\nu}|\phi\rangle=A\left[|\varepsilon\nu\rangle+\int_{-B}^{0}d\varepsilon'\,a(\varepsilon)|\varepsilon'\varepsilon\nu 1\rangle+\int_{-B}^{0}d\varepsilon'\int_{-B}^{\varepsilon'}d\varepsilon''\,b(\varepsilon,\varepsilon')|\varepsilon'\varepsilon''\varepsilon\nu\rangle\right]\ , \tag{5.29}$$

where $|\phi\rangle$ is the "large-degeneracy" ground state (5.16). These states diagonalize the Hamiltonian in the space {(5.17),(5.18),(5.20)}. This is the relevant space for a large N_f, since the states (5.19) and (5.21) only couple with a strength $\tilde{V}/\sqrt{N_f}$ to this space. The states (5.29) have the energy $E_0(N)-\varepsilon$ and they are the only low-lying eigenstates in the studied space with $N-1$ electrons, while there are additional states at higher energies. Using Eqs. (5.3) and (5.6) we find that for $\tau(\varepsilon)\equiv 0$ the states (5.29) give a contribution to the current

$$j_1(\omega+\varepsilon)\equiv\tau^2\rho_v^{(1)}(\varepsilon)=\sum_\nu|\langle\tilde{\varepsilon}\nu|\tau\psi_\nu|\phi\rangle|^2$$
$$=\tau^2A^4\left[a(\varepsilon)\left[1-\int_{-B}^{0}d\varepsilon'\frac{a(\varepsilon')\tilde{V}(\varepsilon')}{2\varepsilon_f+U-\Delta E-\varepsilon-\varepsilon'}\right]-\tilde{V}(\varepsilon)\int_{-B}^{0}d\varepsilon'\frac{[a(\varepsilon')]^2}{2\varepsilon_f+U-\Delta E-\varepsilon-\varepsilon'}\right]^2\ , \tag{5.30}$$

where we have used the result (4.5) for $b(\varepsilon,\varepsilon')$ and replaced $\sqrt{N_f-1}$ by $\sqrt{N_f}$. The solid curve in Fig. 3 shows Eq. (5.30) as a function of U. In the limit $U=\infty$ the two integrals in Eq. (5.30) vanish and we recover the expression (6.23) in paper I,

$$A^4[\tau a(\varepsilon)]^2\ , \tag{5.31}$$

which is the only contribution to the spectrum for $U=\infty$ in the energy range $\Delta E-\varepsilon_f\leq\varepsilon<0$. The shape was discussed in detail in paper I, and the weight was shown to be $\tau^2w(f^0)w(f^1)$ for a singlet ground state in the limit $U\rightarrow\infty$.

For finite U the two integrals in Eq. (5.30) contribute to the spectrum. If $V(\varepsilon)$ does not change sign as a function of ε, all the terms have the same sign and Eq. (5.30) leads to constructive interference. In Fig. 3 the dashed line shows the term $A^4[\tau a(\varepsilon)]^2$ [Eq. (5.31)] and the dotted line shows the contribution

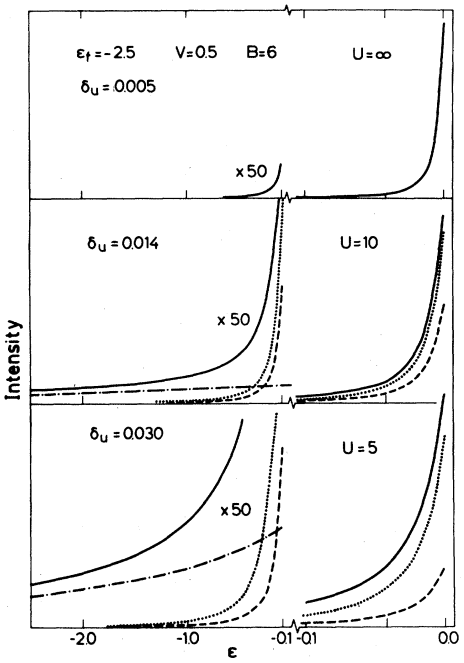

FIG. 3. Various contributions to the valence spectrum as a function of U. The solid curves show Eq. (5.30), which is the only contribution to the valence spectrum for $\varepsilon=0$. The remaining curves show some of the terms in (5.30), namely Eq. (5.31) (dashed), Eq. (5.32) (dotted), and Eq. (5.34) (dashed-dotted). The parameters are $\varepsilon_f=-2.5$ eV, $\tilde{\Delta}=1.2$ eV, and $B=6$ eV. The calculated f^0 weights are 0.02 ($U=\infty$), 0.03 ($U=10$), and 0.03 ($U=5$) and the corresponding f^2 weights are 0, 0.02, and 0.08, respectively. The integrated weights of the curves for $U=5$ are 0.23 (solid), 0.03 (dashed), 0.09 (dotted), and 0.06 (dotted-dashed).

$$\tilde{j}_1(\varepsilon)\equiv A^4[\tau a(\varepsilon)]^2 \times\left[1-\int_{-B}^{0}\frac{a(\varepsilon')\tilde{V}(\varepsilon')}{2\varepsilon_f+U-\Delta E-\varepsilon-\varepsilon'}\right]^2. \quad (5.32)$$

Close to $\varepsilon=0$, Eq. (5.32) gives the main contribution to the spectrum. As shown in Fig. 3, $A^4[\tau a(0)]^2$ is reduced when U is reduced, while $\tilde{j}_1(0)$ stays almost constant. This can be understood using the results of the discussion following Eq. (4.17). In the spin-fluctuation limit and for constant $\tilde{V}(\varepsilon)$ the results for A and I_1 together with Eq. (4.13) lead to

$$\tilde{j}_1(\varepsilon)\approx\frac{\tau^2}{N_f\Delta/\pi}\left[\frac{\delta_u}{\varepsilon-\delta_u}\right]^2 \quad (5.33)$$

for ε close to zero. In Eq. (5.33), $\tilde{j}_1(0)$ is independent of U. For $\varepsilon\ll-\delta_u$ the contribution (5.30) to the PE current is dominated by

$$\tilde{j}_1\equiv A^4\left[-\tau V(\varepsilon)\int_{-B}^{0}d\varepsilon'\frac{[a(\varepsilon')]^2}{2\varepsilon_f+U-\Delta E-\varepsilon-\varepsilon'}\right]^2 \quad (5.34)$$

for the parameters considered in this paper (see Fig. 3).

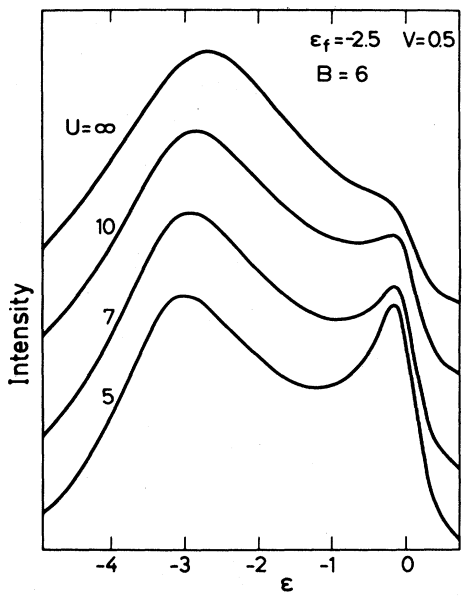

FIG. 4. The f-derived [$\tau(\varepsilon)\equiv0$] valence PE spectrum as a function of U for $\varepsilon_f=-2.5$ eV, $V=0.5$ eV ($\tilde{\Delta}=1.2$ eV), $B=6$ eV, and $N_f=14$. A Lorentzian broadening of 0.5 eV [full width at half maximum (FWHM)] was used. The bottom of the conduction band is at $-B$ ($=-6$ eV).

The reason is that this term falls off on an energy scale $2\varepsilon_f+U-\Delta E=\varepsilon_++\delta_u$, which is much larger than δ_u, which determines the energy variation of $a(\varepsilon)$ [Eq. (4.13)].

Using the results of Sec. IV the expression for $\rho_v(0)$ [Eq. (5.30)] can be simplified in the spin-fluctuation limit to

$$\rho_v(0)\approx\frac{1}{\tilde{\Delta}/\pi}\left[1+(1-\langle P_2\rangle_{\rm mag})\frac{\tilde{\Delta}/\pi}{\varepsilon_+}\right]^2. \quad (5.35)$$

For $B\ll U$ and constant $V(\varepsilon)$ the expression in the larger parentheses is just the f occupancy n_f, and (5.35) shows that the generalized Friedel sum rule[22] is fulfilled. For arbitrary parameters (but $N_f\to\infty$), the more general version of the Friedel sum rule, which involves the *total* locally displaced charge, must be used. As discussed in Appendix C, the expression (5.30) for $\rho_v(0)$ is in agreement with this general version of the sum rule.

When a realistic experimental broadening is introduced (see Fig. 4) the large value of $\rho_v(0)$ cannot be observed, since this broadening is usually larger than δ_u. The integrated weight of the various contributions in Fig. 3 are then more important than the maximum values. The weight of the contribution $\tilde{j}_1(\varepsilon)$, which varies on the energy scale δ_u, is proportional to δ_u [see Eq. (5.33)]. The weight of this onset to the "Kondo peak," seen in the BIS spectrum, therefore can increase or decrease when U is reduced. In Fig. 3(c) the weights of $\tilde{j}_1(\varepsilon)$ (dotted line: 0.09) and $\tilde{\tilde{j}}_1(\varepsilon)$ (dotted-dashed line: 0.06) are comparable. Interference between these two contributions is also important, since the total weight (0.23) is larger than the sum (0.15) of the two individual weights. If V is reduced further, the f^0 weight becomes very small and Eq. (5.34)

gives the main contribution to the weight of Eq. (5.30). This term is entirely due to the f^2 weight in the initial state. To understand why even a relatively small f^2 weight is important for the spectrum, we observe that applying ψ_ν to $|\phi\rangle$ [Eq. (5.6) with $\tau(\varepsilon)\equiv 0$, i.e., f-level photoemission] leads to states $|\varepsilon'\varepsilon\nu 1\rangle$ with two holes and one f electron. These basis states overlap strongly with the low-lying final states for $-\varepsilon_f \gg \tilde{\Delta}$. Applying ψ_ν to the f^1 part of $|\phi\rangle$, on the other hand, leads to states $|\varepsilon\nu\rangle$ with no f electron. For $-\varepsilon_f \gg \tilde{\Delta}$ these states overlap weakly with the low-lying final states and the integrated contribution (5.31) is small. The importance of the f^2 weight in the initial state is further enhanced by the fact that there are two ways of removing an f electron from an f^2 state, but there is just one possibility for an f^1 state.

Figure 4 shows the full valence spectrum, calculated from Eqs. (5.5)—(5.13), with a realistic broadening. The figure illustrates how the integrated weight of the structure at ε_F increases as U is reduced. This effect is quite large although the f^2 weight in Fig. 4 is at most 8%.

Figure 5 shows the valence PE spectrum for $\tau(\varepsilon)\equiv 0$ as a function of V. The weight of the structure close to ε_F depends strongly on V. In contrast to the $U=\infty$ case, however, the structure does not vanish as the f^0 weight goes to zero. For $V=0.3$ the calculated f^0 weight is only 10^{-3}, but the spectrum nevertheless shows a shoulder at ε_F. This is due to the f^2 weight, which in this case is 0.03. For small values of V the f^0 weights quoted in Fig. 5 differ from those in Table VIII, due to the larger basis set in Table VIII.

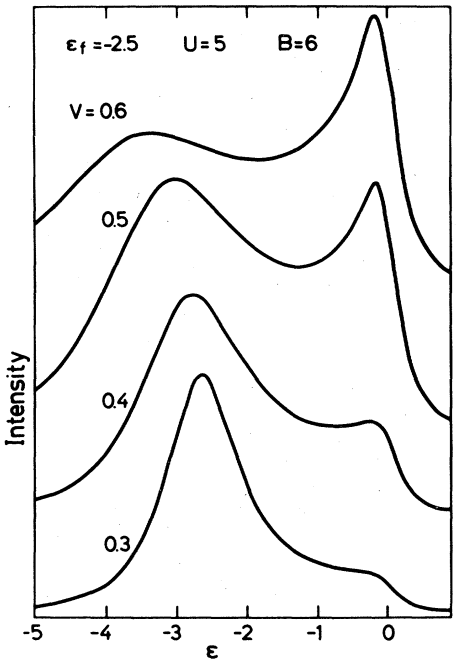

FIG. 5. The f-derived valence PE spectrum as a function of V for $\varepsilon_f=-2.5$ eV, $U=5$ eV, $B=6$ eV, and $N_f=14$. A Lorentzian broadening of 0.5 eV (FWHM) was introduced. The calculated f^0 weights are 0.06 ($V=0.6$ eV and $\tilde{\Delta}=1.7$ eV), 0.03 ($V=0.5$ eV and $\tilde{\Delta}=1.2$ eV), 0.00 ($V=0.4$ eV and $\tilde{\Delta}=0.74$ eV), and 0.00 ($V=0.3$ eV and $\tilde{\Delta}=0.42$ eV), and the corresponding f^2 weights are 0.10, 0.08, 0.05, and 0.03, respectively.

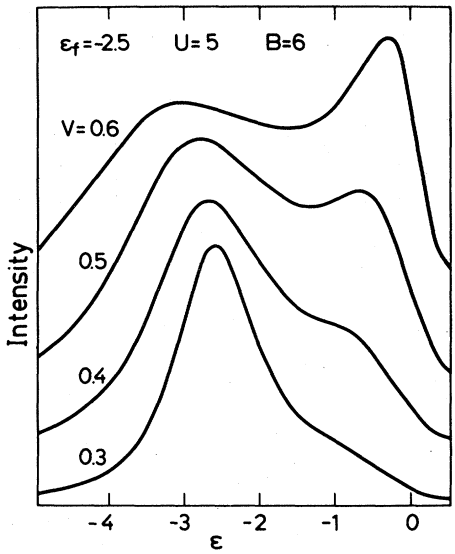

FIG. 6. The f-derived valence PE spectrum as a function of V for the parameters $\varepsilon_f=-2.5$ eV, $U=5$ eV, and $B=6$ eV. The model (5.36) for $[\tilde{V}(\varepsilon)]^2$ was used and a Lorentzian broadening of 0.5 eV (FWHM) was introduced. The calculated values for the f^2 weights were 0.08 ($V=0.6$ eV), 0.06 ($V=0.5$ eV), 0.04 ($V=0.4$ eV), and 0.02 ($V=0.3$ eV), and the corresponding f^0 weights are all smaller than 0.01 due to the small value of $[\tilde{V}(0)]^2$.

In Fig. 6 the spectrum is shown for a more complicated $V(\varepsilon)$,

$$[V(\varepsilon)]^2=\begin{cases} F(\varepsilon)[1-0.8(\varepsilon+1)], & -1\le\varepsilon\le 0 \\ F(\varepsilon), & \text{otherwise} \end{cases} \tag{5.36}$$

where $F(\varepsilon)$ is the semielliptical function defined in Eq. (3.2). In Eq. (5.36), $[V(\varepsilon)]^2$ is reduced to 0.2 of the value of $F(\varepsilon)$ at $\varepsilon=0$ due to the additional linear factor. This shape is considered, since for many Ce compounds with transition elements, the density of states decreases rapidly as the Fermi energy is approached from below. Compared with Fig. 5, the structure close to ε_F is shifted away from ε_F, and this shift increases as V is reduced. This can be understood from formulas (5.30) and (5.34). Because of the reduction of $[\tilde{V}(\varepsilon)]^2$ for $\varepsilon\approx 0$ in Eq. (5.36), the f^0 weight is small, particularly for small values of V. The contribution (5.34) therefore dominates in Eq. (5.30). This term has two factors, one proportional to $[\tilde{V}(\varepsilon)]^2$ and one which decays on the energy scale $2\varepsilon_f+U-\Delta E$. Since this energy scale is several electron volts in Fig. 6, the variation of $[\tilde{V}(\varepsilon)]^2$ between 0 and -1 eV becomes very important. For the form of $[\tilde{V}(\varepsilon)]^2$ in Eq. (5.36), this leads to a structure at ~ -1 eV. Since Eq. (5.30) gives the total spectrum only very close to ε_F, there are, however, additional contributions to the spectrum which partly hide the structure at -1 eV, particularly for large values of V.

In Figs. 3—6 it was assumed that the matrix element $\tau(\varepsilon)$ describing conduction-band emission is zero. In Fig.

7 results are shown for a nonzero $\tau(\varepsilon)$, assuming that $\tau(\varepsilon)$ has the same semielliptical shape as $V(\varepsilon)$. The bottom part of Fig. 7 shows the conduction-band emission only, i.e., the spectrum when the f-emission matrix element τ is zero. Following the normal experimental procedure, we subtract the conduction-band emission from the total spectrum, which gives the solid curves in the upper part of the figure. The dashed curve shows the result when only f emission is considered [$\tau(\varepsilon)\equiv 0$]. The difference between the solid and dashed curves is due to interference between f emission and conduction-band emission. This can be seen from Eqs. (5.14) and (5.15), which lead to cross terms proportional to $\tau\tau(\varepsilon)$. The relative sign of τ and $\tau(\varepsilon)$ is therefore crucial, as is illustrated in Fig. 7. Theoretical and experimental Ce spectra were compared in paper I and in Ref. 7.

To apply the above theory to Pr compounds, one should take into account that these compounds have approximately one more f electron than Ce compounds. For Ce, the low-lying final states, which contribute to the spectrum close to ε_F, have mainly f^1 character. In paper I we therefore found that the spin-orbit splitting leads to an additional structure at ε_F. The low-lying states of Pr have mainly f^2 character, and the introduction of multiplet splitting should lead to additional structure at ε_F. The coefficients in the matrix elements are also changed when the f^0, f^1, and f^2 states appropriate for Ce are replaced by f^1, f^2, and f^3 states appropriate for Pr. We may, nevertheless, obtain some understanding of the Pr spectra by using the simpler theory for Ce with appropriate modifications of ε_f and $\tilde{\Delta}$.

In Fig. 8 we show some results related to Pr. All calculated spectra have a Lorentzian broadening with the half-width

$$\Gamma(\varepsilon)=\Gamma_1\,|\,\varepsilon_F-\varepsilon\,| \tag{5.37}$$

to describe the lifetime broadening. Furthermore, we introduce a Gaussian instrumental broadening. In the inset we show results for $[V(\varepsilon)]^2$ with a broadening as described. The shape of $[V(\varepsilon)]^2$ was adjusted so that the broadened spectrum agrees with the experimental results of Wieliczka *et al.*[28] at $\hbar\omega=32$ eV. At this energy the conduction-band emission dominates over the f emission and this procedure should therefore incorporate density-of-states effects in $[V(\varepsilon)]^2$. This approach entirely neglects that the conduction density of states $\rho(\varepsilon)$ is weighted by a hopping matrix element squared in $[V(\varepsilon)]^2$ and a dipole matrix element squared in photoemission. Without any detailed knowledge about the matrix elements, this, however, appears to be the best procedure. The f spectrum is compared with the experimental results of Parks *et al.*[29] for $Pr_{0.9}Th_{0.1}$, since they have subtracted conduction and inelastic contributions from their spec-

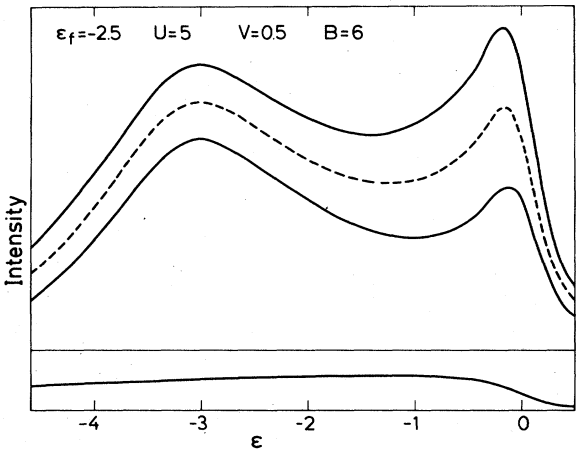

FIG. 7. The valence PE spectrum including both f emission and conduction-band emission as a function of V for $\varepsilon_f=-2.5$ eV, $U=5$ eV, $V=0.5$ eV, $B=6$ eV, and $N_f=14$. A Lorentzian broadening of 0.5 eV was used. The bottom part shows the conduction-band emission ($\tau=0$). The remaining curves show the spectrum after the conduction-band emission has been subtracted (solid curves) and the pure [$\tau(\varepsilon)\equiv 0$] f spectrum (dashed curve). Calculations were performed for both a positive and negative $\tau(\varepsilon)$ to illustrate constructive as well as destructive interference.

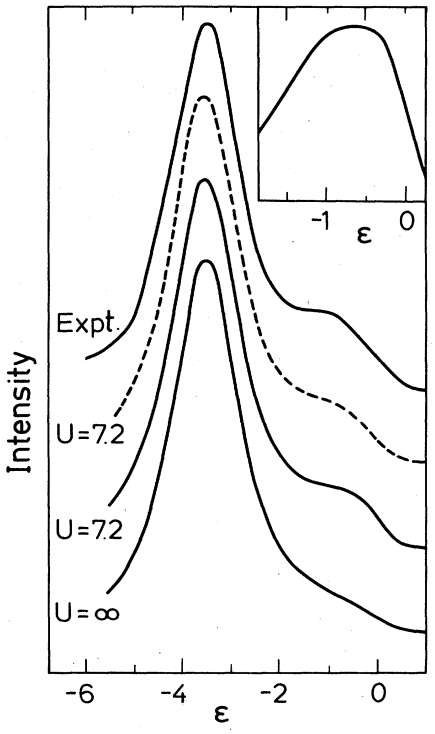

FIG. 8. The conduction- (inset) and f-emission spectra for $\varepsilon_f=-3$, $\Gamma_1=0.2$, and $U=7.2$, as well as $U=\infty$. The average of $\Delta(\varepsilon)$ across the band is 0.02 eV. In addition to the lifetime broadening (5.37), we used a Gaussian broadening for the conduction- and f-emission spectra of 0.25 and 0.60 (FWHM), respectively, to be able to compare with experimental results in Refs. 28 and 29. The dashed curve was obtained by assuming a weak energy dependence for the matrix elements (see text). The f^2 weight for $U=7.2$ is 0.01. All energies are in eV.

trum. Since the f peak at -3.5 eV is below the bottom of the $5d$ band, its width should (essentially) be due to lifetime and instrumental effects. We have therefore adjusted Γ_1 so that the experimental width is reproduced. The value of U was chosen according to the center of the f^3 peak in the Pr BIS spectrum.[30]

Despite the many approximations introduced, the theoretical curve reproduces the experimental results fairly well. This is, in particular, the case if we multiply $[V(\varepsilon)]^2$ by the *ad hoc* factor

$$1-0.4(\varepsilon+1)\ , \tag{5.38}$$

as shown by the dashed curve in Fig. 8. This curve illustrates to what extent the results depend on the assumption that the hopping and dipole matrix elements have the same energy dependence. The dashed curve could be obtained if we assume that the ratio between the dipole and hopping matrix elements increase by $\approx 20\%$ per eV. Since the states at the bottom of the band are generally more extended, it is not surprising if our method of estimating $[V(\varepsilon)]^2$ leads to too small values for these states. Repetition of the calculations in Fig. 8 with a small broadening shows that the plateau for small ε actually is due to two structures, one at $\varepsilon\sim -0.25$ eV and one at $\varepsilon\sim -1$ eV, as was observed experimentally in Ref. 28. The introduction of the factor (5.38) reduces the weight of the structure at $\varepsilon\sim -0.25$ eV, and in Fig. 8 this appears as a shift in energy of the plateau.

It is interesting to consider the results for $U=\infty$ in Fig. 8. Although the weight at ~ -1 eV is reduced, the spectrum clearly deviates from a Lorentzian located at -3.5 eV. The $U=\infty$ case was discussed in paper I, and it was shown that the valence spectrum of the $N_f=\infty$ model can be written as

$$\rho_v^{U=\infty}(\varepsilon)=\frac{A^2}{\pi}\int_{-B}^{0} d\varepsilon'[a(\varepsilon')]^2 \mathrm{Img}(\varepsilon-\varepsilon'-i0)\ , \tag{5.39}$$

where $(1/\pi)\mathrm{Img}(\varepsilon-i0)$ is the spectrum of a nondegenerate model ($N_f=1$) with the hopping matrix element $\tilde{\tilde{V}}(\varepsilon)=\tilde{V}(\varepsilon)=\sqrt{N_f}V(\varepsilon)$ for $\varepsilon\le\varepsilon_F=0$ and $\tilde{\tilde{V}}(\varepsilon)=0$ for $\varepsilon>\varepsilon_F$. The sharp cutoff in $\tilde{\tilde{V}}(\varepsilon)$ at $\varepsilon=\varepsilon_F$ leads to a pole in $g(\varepsilon)$ and a continuous rise in $\rho_v^{U=\infty}(\varepsilon)$ as ε approaches ε_F. The weight of the pole in $g(\varepsilon)$ is given by $w(f^0)$. This weight is less than 10^{-3} in Fig. 8 and can be neglected. Furthermore, $A^2[a(\varepsilon)]^2$ is to a good approximation a δ function since the Kondo temperature δ_u is very small [see Eq. (4.13)]. In this case ($-\varepsilon_f\gg\tilde{\Delta}$ and $U=\infty$) we can therefore describe the spectrum by an $N_f=1$ model, if the hopping matrix elements $\tilde{\tilde{V}}(\varepsilon)$ are used. In such a model the hybridization between the f level and the conduction states at $\varepsilon\sim -1$ eV leads to weight in this energy region, as is illustrated by the $U=\infty$ curve in Fig. 8. An increase of $\tilde{\Delta}$ would enhance the weight at $\varepsilon\sim -1$ eV and the $U=\infty$ curve would give a closer agreement with experiment. Such hybridization effects have been discussed earlier and emphasized by Allen[31] in the context of rare-earth compounds. This effect becomes more important if

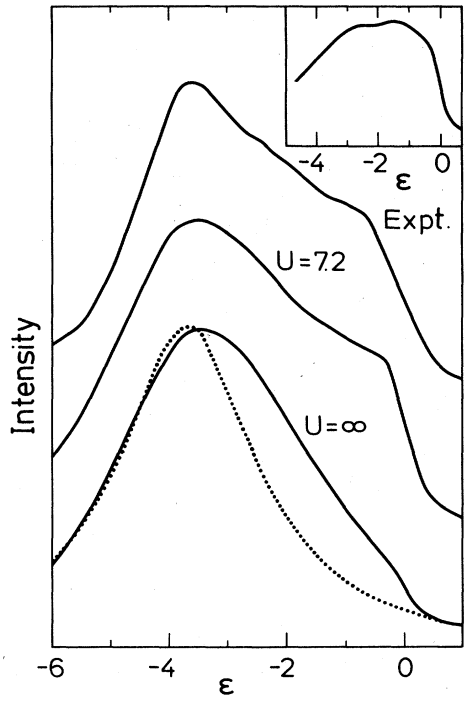

FIG. 9. The conduction- (inset) and f-emission spectra for $\varepsilon_f=-3.4$, $\Gamma_1=0.2$, and $U=7.2$, as well as $U=\infty$. The average of Δ across the band is 0.04 eV. In addition to the lifetime broadening (5.37), we used a Gaussian broadening of 0.60 FWHM. The experimental curve is from Ref. 32. As in Ref. 32, we have also plotted a Lorentzian (dotted) centered at $\varepsilon=-3.7$. The f^2 weight for $U=7.2$ is 0.03. All energies are in eV.

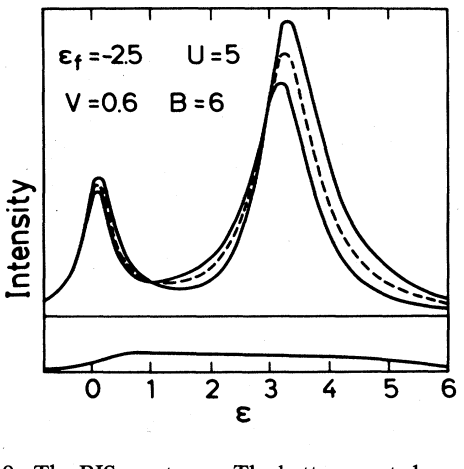

FIG. 10. The BIS spectrum. The bottom part shows the pure conduction contribution [$\tau(\varepsilon)\neq 0$, $\tau=0$]. The dashed curve shows the pure f spectrum [$\tau\neq 0$, $\tau(\varepsilon)\equiv 0$], and the solid curves show the spectrum with both types of transitions [$\tau\neq 0$, $\tau(\varepsilon)\neq 0$] minus the pure conduction spectrum. Both $\tau(\varepsilon)>0$ and $\tau(\varepsilon)<0$ are treated. The parameters are $V=0.6$ eV ($\tilde{\Delta}=1.7$ eV), $U=5$ eV, $B=6$ eV, and $N_f=14$. A Lorentzian broadening of 0.6 eV (FWHM) was used.

the f level falls in the middle of a large conduction density of states, as is often the case for Pr compounds containing transition elements. This is illustrated in $PrRu_2$ in Fig. 9. The results in this figure were obtained in the same way as in Fig. 8. The agreement between theory and experiment is good. The comparison between the $U=\infty$ curve and the Lorentzian (dotted curve) illustrates that hybridization effects are of importance.

The part of the valence spectrum which lies above the Fermi energy can experimentally be sampled by BIS and is given by $\mathrm{Img}^{>}(\varepsilon-i0)/\pi$, where $g^{>}(z)$ was defined in (5.14). The BIS spectrum including double occupancy was discussed in paper I and in Ref. 7 for $\tau(E)\equiv 0$. We therefore present only a short discussion of the form of the spectrum for $\tau(E)\equiv 0$ and some numerical results for $\tau(E)\neq 0$. As mentioned before, it is necessary to use a larger basis for the ground and "intermediate" states in the BIS calculation. To understand the gross features of the BIS spectrum, on the other hand, it is sufficient to use the ground state (5.16). To calculate the resolvent matrix element in Eq. (5.14), we then use a state with one f electron and states with two f electrons and one conduction hole. A straightforward calculation then yields, for $\tau(E)\equiv 0$,

$$g^{>}_{(0)}(z)=\tau^2 A^2\left[\frac{1}{z+\Delta E-\varepsilon_f+N_f\tilde{\Gamma}(-z-\Delta E+2\varepsilon_f+U)}\left[1+\int_{-B}^{0}\frac{\tilde{V}(\varepsilon)a(\varepsilon)}{z+\Delta E-2\varepsilon_f-U+\varepsilon}d\varepsilon\right]^2+\int_{-B}^{0}\frac{[a(\varepsilon)]^2}{z+\Delta E-2\varepsilon_f-U-\varepsilon}d\varepsilon\right], \tag{5.40}$$

where we have replaced N_f-1 by N_f. In this (crude) approximation the spectrum shows a sharp f^1 peak at $z=\delta_u$ and an f^2 continuum starting at the energy $2\varepsilon_f+U-\Delta E=\varepsilon_+ +\delta_u$. The residue R_1 of the f_1 peak is given by

$$R_1=\tau^2\langle P_0\rangle(1-\langle P_2\rangle_{\mathrm{mag}})\left[1-\int_{-B}^{0}\frac{\tilde{V}(\varepsilon')a(\varepsilon')}{\varepsilon_+-\varepsilon'}d\varepsilon'\right]\approx\frac{\delta_u}{\tilde{\Delta}/\pi}, \tag{5.41}$$

where the second relation holds in the spin-fluctuation limit. In the improved version of the theory, with basis states as described below Eq. (5.28), this peak is broadened and the part $\tilde{j}_1(\varepsilon)$ [Eq. (5.32)] of the PE current can be interpreted as the "onset" to the f^1 peak, i.e., in the limit $N_f=\infty$, $j_1(\varepsilon)$ [Eq. (5.30)] joins smoothly to the BIS current $N_f\mathrm{Img}^{>}(\varepsilon-i0)/\pi$.

In Fig. 10 we show results for BIS including interference. The figure illustrates that interference effects can change both the relative weights of the peaks and the peak shapes. The importance of interference effects clearly depends on the relative size of τ and $\tau(\varepsilon)$, and estimates of this size would be of great interest.

VI. CONCLUDING REMARKS

We have presented new methods for calculating the f occupancy, the ground-state energy, and the susceptibility of the Anderson impurity model at $T=0$. The calculations include f^0, f^1, and f^2 configurations and are based on the idea that $1/N_f$ can be treated as a small parameter, where N_f is the degeneracy of the f level. Even for $N_f=1$ and $N_f=2$ the method was shown to give accurate results for the f occupancy and the total energy. We have also presented a new method for calculating the valence spectrum using a time-dependent formalism. In this method it is relatively straightforward to include double occupancy of the f level also in the valence photoemission calculation. In a previous publication[10] we used such parameters ($2\varepsilon_f+U>0$) that the f^0 weight was larger than the f^2 weight and $n_f<1$. Here we focus on the "symmetric" parameters $2\varepsilon_f+U=0$. For $N_f>2$ the f^2 weight can then be much larger than the f^0 weight and $n_f\geq 1$. We find that the susceptibility is mainly influenced by the f^0 weight, while for the valence spectrum the f^2 weight is also important. As the f level is pulled down far below the Fermi energy ε_F, the f^0 weight decreases rapidly and the susceptibility grows correspondingly. At the same time the valence spectrum develops a well-defined peak close to ε_f, but a substantial amount of spectral weight remains in a structure close to ε_F: If the conduction density of states has an appreciable structure in the neighborhood of ε_F, as is often the case for compounds containing transition metals, the low-binding-energy structure can be located below ε_F.

We have also studied the effects of interference between f emission and conduction-band emission in model calculations. To determine the importance of these effects, it would be of great interest to make realistic estimates of the matrix elements involved [τ, $\tau(\varepsilon)$]. It should also be important to obtain better understanding of the hopping matrix elements $V(\varepsilon)$, since the energy dependence of $V(\varepsilon)$ can influence the f spectrum substantially.

ACKNOWLEDGMENTS

We want to thank J. W. Allen for many useful discussions and provocative questions, as well as for pointing out the possible importance of double occupancy for the valence photoemission spectrum.

APPENDIX A

Below we describe a variational method, intended for $N_f=2$, which has been used as a comparison to and test

of the $1/N_f$ method described in Sec. II. The method is a direct generalization of a projection-operator method proposed earlier.[33] The starting point is the Hartree-Fock solution $|\psi_{\rm HF}(\alpha,n_0)\rangle$ of a model problem

$$H=\sum_\sigma \left[\int d\varepsilon\, \varepsilon\psi^\dagger_{\varepsilon\sigma}\psi_{\varepsilon\sigma}+(\varepsilon_f+Un_0)\psi^\dagger_\sigma\psi_\sigma \right]+\alpha V\ , \tag{A1}$$

where

$$V=\sum_\sigma \int d\varepsilon[V(\varepsilon)\psi^\dagger_\sigma\psi_{\varepsilon\sigma}+\text{H.c.}]\ . \tag{A2}$$

The quantities α and n_0 are treated as variational parameters below. We define the operators

$$P_0=(1-n_\uparrow)(1-n_\downarrow)\ , \tag{A3}$$

$$P_1=n_\uparrow(1-n_\downarrow)+n_\downarrow(1-n_\uparrow)\ , \tag{A4}$$

$$P_2=n_\uparrow n_\downarrow\ , \tag{A5}$$

and form a variational expression for the ground state,

$$\begin{aligned}|\phi\rangle=&\sum_{i=0}^{2}\lambda_i P_i\,|\psi_{\rm HF}(\alpha,n_0)\rangle\\&+(\lambda_3P_0+\lambda_4P_2)VP_1\,|\psi_{\rm HF}(\alpha,n_0)\rangle\\&+\lambda_5VP_0\,|\psi_{\rm HF}(\alpha,n_0)\rangle+\lambda_6VP_2\,|\psi_{\rm HF}(\alpha,n_0)\rangle\ .\end{aligned} \tag{A6}$$

The expectation value of the true Hamiltonian (1.1) is calculated and the total energy is minimized for fixed values of α and n_0. This gives an energy $E(\alpha,n_0)$, which is minimized with respect to α and n_0. The form of (A6) was discussed in Ref. 33. Compared with Ref. 33, we have added the terms containing λ_5 and λ_6 to further improve the accuracy.

APPENDIX B

Below we describe a method for calculating the magnetic susceptibility including double occupancy of the f level. Since we are mainly interested in the qualitative features of the susceptibility, we neglect the spin-orbit splitting. In the Hamiltonian (1.1) we add a term ($N_f=2j+1$)

$$H=\sum_{\nu=-j}^{j}(-\nu K)\psi^\dagger_\nu\psi_\nu\equiv -KS_Z\ , \tag{B1}$$

which describes the coupling to an external magnetic field K. We obtain the static susceptibility as the $z=0$ limit of the dynamical susceptibility $\chi(z)$,

$$\chi(z)=\left\langle\phi_0\left|S_Z\frac{1}{z+H-E_0}S_Z\right|\phi_0\right\rangle+\left\langle\phi_0\left|S_Z\frac{1}{-z+H-E_0}S_Z\right|\phi_0\right\rangle\equiv G_S(z)+G_S(-z)\ . \tag{B2}$$

We restrict our discussion to the limit of large degeneracy and use the "first-row" ground state (4.1). To calculate the resolvent matrix element $G_S(z)$ we introduce magnetic states [see Eq. (4.8)] with a special choice for the C_ν, dictated by the form of S_Z,

$$|\varepsilon,S_Z\rangle:=\frac{1}{\sqrt{C_0}}\sum_\nu \nu\psi^\dagger_\nu\psi_{\varepsilon\nu}\,|0\rangle\ , \tag{B3}$$

$$|\varepsilon,\varepsilon' S_Z\rangle:=\frac{1}{\sqrt{C_0}}\frac{1}{\sqrt{N_f-1}}\sum_{\substack{\nu,\nu'\\ \nu\neq\nu'}}\psi^\dagger_\nu\psi_{\varepsilon\nu}\nu'\psi^\dagger_{\nu'}\psi_{\varepsilon'\nu'}\,|0\rangle\ , \tag{B4}$$

with

$$C_0=\sum_\nu \nu^2=\tfrac{1}{3}j(j+1)(2j+1)\ . \tag{B5}$$

Using

$$S_Z\,|\phi_0\rangle=A\left[\frac{C_0}{N_f}\right]^{1/2}\left[\int_{-B}^{0}a(\varepsilon)\,|\varepsilon,S_Z\rangle d\varepsilon-\int_{-B}^{0}d\varepsilon\int_{-B}^{0}d\varepsilon'\frac{\tilde V(\varepsilon)a(\varepsilon')+\tilde V(\varepsilon')a(\varepsilon)}{2\varepsilon_f+U-\Delta E-\varepsilon-\varepsilon'}\,|\varepsilon,\varepsilon' S_Z\rangle\right]\ , \tag{B6}$$

it follows that $\chi(z)$ can be expressed in terms of resolvent matrix elements of the states (B3) and (B4). To leading order in $1/N_f$, these states have also to be used as the intermediate states in the calculation. As the calculation is rather straightforward we only quote the final result

$$G_S(0)=A^2\tfrac{1}{3}j(j+1)\left\{\int_{-B}^{0}d\varepsilon\frac{1}{\varepsilon_f-\varepsilon-\Delta E-\overline{\Gamma}(2\varepsilon_f+U-\Delta E-\varepsilon)}\right.$$
$$\times\left[a(\varepsilon)^2\left[1+\int_{-B}^{0}\frac{[\widetilde{V}(\varepsilon_1)]^2}{(2\varepsilon_f+U-\Delta E-\varepsilon-\varepsilon_1)^2}d\varepsilon_1\right]^2\right.$$
$$+2a(\varepsilon)\widetilde{V}(\varepsilon)\int_{-B}^{0}\frac{\widetilde{V}(\varepsilon_1)a(\varepsilon_1)}{(2\varepsilon_f+U-\Delta E-\varepsilon-\varepsilon_1)^2}d\varepsilon_1\left[1+\int_{-B}^{0}\frac{[\widetilde{V}(\varepsilon_1)]^2}{(2\varepsilon_f+U-\Delta E-\varepsilon-\varepsilon_1)^2}d\varepsilon_1\right]$$
$$\left.+[\widetilde{V}(\varepsilon)]^2\int_{-B}^{0}\frac{\widetilde{V}(\varepsilon_1)a(\varepsilon_1)}{(2\varepsilon_f+U-\Delta E-\varepsilon-\varepsilon_1)^2}d\varepsilon_1\right]$$
$$\left.+2\int_{-B}^{0}d\varepsilon\int_{-B}^{0}d\varepsilon'\frac{[\widetilde{V}(\varepsilon)]^2[a(\varepsilon')]^2+\widetilde{V}(\varepsilon)\widetilde{V}(\varepsilon')a(\varepsilon)a(\varepsilon')}{(2\varepsilon_f+U-\Delta E-\varepsilon-\varepsilon')^3}\right\}.$$

In the "spin-fluctuation limit" the dominating contribution is given by that part of the first integral for which the integrand is proportional to $[a(\varepsilon)]^2$. Using (4.11) and (4.13) then leads to the approximate result for χ_0 quoted in Sec. IV [Eq. (4.18)]. The frequency behavior of the dynamical susceptibility will be discussed elsewhere.

APPENDIX C

In this appendix we show that in the limit $N_f=\infty$ the solution for the valence spectral function $\rho_v(\varepsilon)$ [Eq. (5.30)] fulfills the generalized Friedel sum rule[22] (FSR) for arbitrary parameters and not just for the special case discussed in Sec. V.

For arbitrary N_f the spectral function $\rho_\nu(\varepsilon)$ is defined as

$$\rho_\nu(\varepsilon)\equiv\frac{1}{\pi}\mathrm{Im}g_\nu(\varepsilon-i0)$$
$$\equiv\frac{1}{\pi}\mathrm{Im}\langle\phi_0|\left[\psi_\nu^\dagger\frac{1}{\varepsilon-i0-E_0+H}\psi_\nu+\psi_\nu\frac{1}{\varepsilon-i0-H+E_0}\psi_\nu^\dagger\right]|\phi_0\rangle\ . \quad \text{(C1)}$$

For the Hamiltonian (1.1) and arbitrary N_f, the FSR is given by

$$\rho_\nu(\varepsilon_F)=\frac{1}{\pi\Delta(\varepsilon_F)}\sin^2[\pi(n_\nu+\delta n_{\mathrm{loc},\nu})]\ , \quad \text{(C2)}$$

where $n_\nu=n_f/N_f$ is the f-level occupancy in the νth channel. The locally induced charge $\delta n_{\mathrm{loc},\nu}$ around the impurity in the νth channel is given by

$$\delta n_{\mathrm{loc},\nu}=-\frac{1}{\pi}\mathrm{Im}\int_{-\infty}^{\varepsilon_F}\frac{\partial\Gamma(\varepsilon-i0)}{\partial\varepsilon}g_\nu(\varepsilon-i0)d\varepsilon\ , \quad \text{(C3)}$$

where, in contrast to $\widetilde{\Gamma}(z)$ [Eq. (4.4)], $\Gamma(z)$ is defined as

$$\Gamma(z)\equiv\int_{-B}^{B}\frac{[V(\varepsilon)]^2}{z-\varepsilon}d\varepsilon\ . \quad \text{(C4)}$$

The FSR follows from particle number conservation and the Fermi-liquid property $\mathrm{Im}\Sigma_\nu(\varepsilon_F\pm i0)=0$, where $\Sigma_\nu(z)$ is the self-energy defined by

$$g_\nu(z)\equiv[z-\varepsilon_\nu-\Gamma(z)-\Sigma_\nu(z)]^{-1}\ .$$

In the limit of large degeneracy N_f, the sine function can be replaced by its argument and we obtain, in the absence of an external field,

$$\rho_v(\varepsilon_F)=\frac{\pi}{\widetilde{\Delta}(\varepsilon_F)}(n_f+\delta n_{\mathrm{tot}})^2\ , \quad \text{(C5)}$$

where we have defined $\rho_f(\varepsilon)\equiv N_f\rho_\nu(\varepsilon)$ and $\delta n_{\mathrm{tot}}\equiv N_f\delta n_{\mathrm{loc},\nu}$. The same form of the FSR [Eqs. (C2) and (C5)] also holds if one would include a three-body interaction term,

$$U_{(3)}\sum_{\substack{\nu_1,\nu_2,\nu_3\\ \nu_1>\nu_2>\nu_3}}n_{\nu_1}n_{\nu_2}n_{\nu_3}\ ,$$

in the Hamiltonian (1.1). Our restriction to, at most, double occupancy of the f level, would no longer be an approximation if we included such a term in the Hamiltonian and studied the limit $U_{(3)}=\infty$. The FSR (C5) should therefore be exactly fulfilled by our result for $\rho_v(\varepsilon_F)=\rho_v^1(\varepsilon_F)$ [Eq. (5.30)].

For an infinitely broad, flat band

$$\Gamma(z)=-i\Gamma\,\mathrm{sgn}(\mathrm{Im}z)\ ,$$

the locally induced charge vanishes, $\delta n_{\mathrm{loc},\nu}=\delta n_{\mathrm{tot}}=0$, and the FSR (C5) implies a "consistency relation" for the function $a(\varepsilon)$, as both $n_f=\langle P_1\rangle+2\langle P_2\rangle$ [see Eq. (4.17)] and $\rho_v(\varepsilon_F)$ [Eq. (5.30)] can be expressed in terms of $a(\varepsilon)$. For an arbitrary $\Gamma(z)$, Eq. (C3) has to be used to calculate the locally induced charge. In the limit $N_f\to\infty$ ($N_f\Delta=$const) the function $\Gamma(z)$ in (C3) is of order $1/N_f$. To obtain $\delta n_{\mathrm{loc},\nu}$ to order $1/N_f$, i.e., δn_{tot} to order $(1/N_f)^0$, it is therefore sufficient to use an approximation

for $g_\nu(\varepsilon)$ which is correct to order $(1/N_f)^0$. If we set the factor τ^2 equal to unity, this is just given by the "crude" approximation (5.40) to the BIS spectrum. As the function $g^>_{(0)}(\varepsilon - i0)$ has a vanishing imaginary part for $\varepsilon < \varepsilon_F$, one obtains, to order $(1/N_f)^0$,

$$\delta n_{\rm tot} = -\frac{1}{\pi}\int_{-\infty}^{\varepsilon_F} \frac{\partial \tilde{\Delta}(\varepsilon)}{\partial \varepsilon} g^>_{(0)}(\varepsilon)\, d\varepsilon$$

$$= -[\tilde{V}(\varepsilon_F)]^2 g^>_{(0)}(\varepsilon_F) + \int_{-\infty}^{\varepsilon_F} [\tilde{V}(\varepsilon)]^2 \frac{\partial g^>_{(0)}(\varepsilon)}{\partial \varepsilon} d\varepsilon \,. \tag{C6}$$

Using (4.3), $g^>_0(\varepsilon)$ can be expressed in terms of $a(\varepsilon)$,

$$g^>_{(0)}(\varepsilon) = \frac{A^2}{\tilde{V}(\varepsilon)} \left[a(\varepsilon) \left[1 + \int_{-B}^{0} \frac{a(\varepsilon')\tilde{V}(\varepsilon')}{\varepsilon+\varepsilon'+\Delta E - 2\varepsilon_f - U} d\varepsilon' \right] + \tilde{V}(\varepsilon) \int_{-B}^{0} \frac{[a(\varepsilon')]^2}{\varepsilon+\varepsilon'+\Delta E - 2\varepsilon_f - U} d\varepsilon' \right] . \tag{C7}$$

Differentiating $g^>_0(\varepsilon)$ with respect to ε [using (5.40)], one easily shows that the integral in the second equality in (C6) is just $-n_f$ [Eq. (4.17)]. Comparison of (C7) with (5.30) then shows that the FSR (C5) is fulfilled without any additional assumptions about the parameters of the system.

---

*Present address: Institut für Theoretische Physik, Universität Göttingen, D-3400 Göttingen, West Germany.

[1] P. W. Anderson, Phys. Rev. **124**, 41 (1961).

[2] H. A. Bethe, Z. Phys. **71**, 205 (1931); N. Andrei, Phys. Rev. Lett. **45**, 379 (1980); P. B. Wigman, Pis'ma Zh. Eksp. Teor. Fiz. **31**, 392 (1980) [JETP Lett. **31**, 364 (1980)]; J. Phys. F **4**, L169 (1974).

[3] P. Schlottmann, Phys. Rev. Lett. **50**, 1697 (1983); E. Ogievetski, A. M. Tsvelick, and P. B. Wiegmann, J. Phys. C **16**, L797 (1983).

[4] B. Johansson, Philos. Mag. **30**, 469 (1974); J. Phys. F **4**, L169 (1974).

[5] J. F. Herbst and J. W. Wilkins, Phys. Rev. Lett. **43**, 1760 (1979); J. F. Herbst, R. E. Watson, and J. W. Wilkins, Phys. Rev. B **13**, 1439 (1976); **17**, 3089 (1978); J. K. Lang, Y. Baer, and P. A. Cox, Phys. Rev. Lett. **42**, 74 (1979).

[6] J. W. Allen, S.-J. Oh, I. Lindau, J. M. Lawrence, L. I. Johansson, and S. B. Hagström, Phys. Rev. Lett. **46**, 1100 (1981); M. Croft, J. H. Weaver, D. J. Peterman, and A. Franciosi, *ibid.* **46**, 1104 (1981).

[7] J. C. Fuggle, F. U. Hillebrecht, J.-M. Esteva, R. C. Karnatak, O. Gunnarsson, and K. Schönhammer, Phys. Rev. B **27**, 4637 (1983); J. C. Fuggle, F. U. Hillebrecht, Z. Zołnierek, R. Lasser, Ch. Freiburg, O. Gunnarsson, and K. Schönhammer, *ibid.* **27**, 7330 (1983); F. U. Hillebrecht, J. C. Fuggle, G. A. Sawatzky, M. Campagna, O. Gunnarsson, and K. Schönhammer, *ibid.* **30**, 1777 (1984); O. Gunnarsson, K. Schönhammer, J. C. Fuggle, F. U. Hillebrecht, J.-M. Esteva, R. C. Karnatak, and B. Hillebrand, *ibid.* **28**, 7330 (1983).

[8] H. R. Krishna-murthy, J. W. Wilkins, and K. G. Wilson, Phys. Rev. B **21**, 1003 (1980); **21**, 1044 (1980).

[9] See, e.g., N. Kawakami and A. Okiji, Phys. Lett. **86A**, 483 (1981); J. Phys. Soc. Jpn. **51**, 1145 (1982).

[10] O. Gunnarsson and K. Schönhammer, Phys. Rev. B **28**, 4315 (1983); Phys. Rev. Lett. **50**, 604 (1983).

[11] T. V. Ramakrishnan, in *Valence Fluctuations in Solids,* edited by L. M. Falicov, W. Hanke, and M. P. Maple (North-Holland, Amsterdam, 1981), p. 13; T. V. Ramakrishnan and K. Sur, Phys. Rev. B **26**, 1798 (1982); P. W. Anderson, in *Valence Fluctuations in Solids,* p. 451.

[12] N. Read and D. M. Newns, J. Phys. C **16**, 3273 (1983); F. C. Zhang and T. K. Lee, Phys. Rev. B **28**, 33 (1983); J. W. Rasul and A. C. Hewson, J. Phys. C **16**, L933 (1983); **17**, 2555 (1984); **17**, 3337 (1984).

[13] Y. Kuramoto, Z. Phys. B **53**, 37 (1983); P. Coleman, Phys. Rev. B **29**, 3035 (1984); T. K. Lee and F. C. Zhang, Phys. Rev. B **30**, 1556 (1984); H. Kojima, Y. Kuramoto, and M. Tachiki, Z. Phys. B **54**, 293 (1984).

[14] C. M. Varma and Y. Yafet, Phys. Rev. B **13**, 2950 (1976).

[15] See, e.g., J. H. Wilkinson, *The Algebraic Eigenvalue Problem* (Clarendon, Oxford, 1965), p. 617.

[16] The lowest eigenvalue of H always has a finite separation to the next eigenvalue. If we consider the parameters for $\varepsilon_f = -1$ in Table I and use the basis set or $a+c+d$ together with $N_E = 41$ and $\alpha = 0.2$ (see Ref. 18), the two lowest eigenvalues are -1.4076 and -1.3804. For $n = 35$ [Eq. (2.12)] the ground-state energy and the f occupancy are converged in the third decimal place.

[17] In an earlier application [O. Gunnarsson and P. Johansson, Int. J. Quant. Chem. **10**, 307 (1976)] of this method we found a $N^{3/2}$ dependence. In that case the upper bound on the spectrum of H depended strongly on N, which was reflected in a strong N dependence for the lower bound, a, of the transformed spectrum. This led to an additional factor $\sqrt{N}$ in the computational work.

[18] For the larger basis sets, the results may have numerical errors in the last digit. The calculations require a discretization of the energy mesh, and in some calculations the results may not be fully converged with respect to the number of mesh points. We have used an exponential energy mesh, $\varepsilon = \pm[\alpha - \exp(x)]$; $\ln\alpha \le x \le \ln(\alpha + B)$, which heavily weights the energies close to ε_F, and the integrals were performed according to Simpson's rule. For the largest basis set (g in Fig. 1) the number of mesh points, N_E, in the energy range $[-B, B]$ was limited to $N_E = 49$ for $N_f = 1$ and $N_E = 29$ for $N_f > 1$.

[19] P. W. Anderson, Phys. Rev. Lett. **18**, 1049 (1967); D. R. Hamann, *ibid.* **26**, 1030 (1971); K. Yamada and K. Yosida, Prog. Theor. Phys. **59**, 1061 (1978); **62**, 363 (1979).

[20] This effect is not obvious from a comparison of the $N_f = 1$ and $N_f = 6$ results, since some of the basis states do not enter in the $N_f = 1$ calculation.

[21] We define a phase shift $\delta = \pi n_f / N_f$ and insert it in Anderson's estimate (Ref. 19) S for the overlap between the perturbed and unperturbed ground states. We obtain $S \approx \exp[-n_f^2 \ln N/(3N_f)]$. With $n_f = 0.6$, $N_f = 14$, and $N = 10^{22}$, we find $S = 0.65$. This suggests that for large values of N_f the orthogonality catastrophe becomes important only for very large N.

[22]D. C. Langreth, Phys. Rev. **150**, 516 (1966); R. M. Martin, Phys. Rev. Lett. **48**, 362 (1982). F. D. M. Haldane, in *Valence Fluctuations in Solids,* see Ref. 11, p. 153.
[23]E. Müller-Hartmann (unpublished).
[24]P. Nozières and C. T. de Dominicis, Phys. Rev. **178**, 1097 (1969).
[25]K. Schönhammer and O. Gunnarsson, Solid State Commun. **23**, 691 (1977); **26**, 399 (1978).
[26]R. Haydock, in *Solid State Physics,* edited by H. Ehrenreich, D. Turnbull, and F. Seitz (Academic, New York, 1980), Vol. 35, p. 215.
[27]See, e.g., L. Hedin and S. Lundqvist, in *Solid State Physics,* edited by H. Ehrenreich, D. Turnbull, and F. Seitz (Academic, New York, 1969), Vol. 23, p. 1.
[28]D. M. Wieliczka, C. G. Olson, and D. W. Lynch, Phys. Rev. Lett. **52**, 2180 (1984).
[29]R. D. Parks, S. Raaen, M. L. de Boer, and Y.-S. Chang (unpublished).
[30]J. K. Lang, Y. Baer, and P. A. Cox, J. Phys. F **11**, 121 (1981).
[31]J. W. Allen (private communication), and as quoted in Ref. 28.
[32]R. D. Parks, S. Raaen, M. L. den Boer, Y. S. Chang, and G. P. Williams, Phys. Rev. Lett. **52**, 2176 (1984).
[33]K. Schönhammer, Phys. Rev. B **13**, 4336 (1976); Z. Phys. B **21**, 389 (1975).